Table 3 Basic information of 290 patients with CTDs according to the presence of anti-hnRNP-K antibodies

Variable	Positive (n = 69)	Negative (n = 221)	P value*
Age, mean (s.d.), years	52.4 (15.6)	53.3 (15.4)	0.3613
Gender (F:M), n:n	61:8	192:29	0.8383
Smoking, % (n/N)	18.9 (10/53)	31.6 (56/177)	0.0841
RP, % (n)	88.4 (61)	64.3 (142)	0.0001
ANA positivity, % (n/N)	94.0 (63/67)	93.1 (203/218)	1.0000
Anti-U1-RNP, % (n/N)	26.5 (18/68)	23.1 (50/166)	0.6255
Anti-SSA/Ro positivity, % (n/N)	27.9 (19/68)	23.6 (52/220)	0.5202

*Univariate analysis using the Mann-Whitney U test or Fisher's exact test. N: the number of available patients (varies according to the number of available observations). hnRNP-K: heterogeneous nuclear ribonucleoprotein K.

RA (31% and 24%, respectively), although the co-morbidity of RP in these patients was not described in this report [28]. Autoantibodies to other hnRNPs such as hnRNP-H1 [29], -B1 and -F [30] have also been reported as possible diagnostic markers of CTDs, but their relevance to RP has not been examined.

Although anti-hnRNP-K antibody was identified initially using sera from patients with SSc-related RP, this autoantibody was also detected in sera from RP patients with other CTDs. Notably, anti-hnRNP-K antibody levels in RP patients secondary to SSc, SLE and MCTD were significantly higher than in HCs. In addition, the prevalence of anti-hnRNP-K antibody in SSc patients with RP (26.5%), SLE patients with RP (42.1%) and MCTD patients with RP (40.0%) was markedly higher than in their RP-negative counterparts (9.4%, 9.3% and 0%, respectively) and in primary RP patients (0%). Moreover, anti-hnRNP-K autoantibody was not associated with smoking, which was believed to be a cause of blood vessel narrowing [31], nor with the presence of anti-U1-RNP and ACAs, which are highly related to MCTD and SSc, respectively [32, 33]. Thus these results suggest that anti-hnRNP-K antibody is particularly relevant to CTD-related secondary RP, but not to a single CTD or primary RP. Our findings should be replicated in a larger study.

The pathogenesis of RP likely involves various abnormalities in the vascular, neural and intravascular systems [4]. At present, it remains to be determined whether anti-hnRNP-K autoantibody detected by our ELISA system can bind to hnRNP-K on vascular endothelial cells in vivo. In addition, it is unknown whether this autoantibody contributes to the pathogenesis. Because our cohort of patients includes only a limited number of severe RP patients who experienced hospitalization and/or digit loss, it is unknown whether anti-hnRNP-K antibody correlates with the severity of RP. However, it is tempting to speculate that following cold stimulation, anti-hnRNP-K autoantibody may promote antibody-dependent pathogenesis by inducing vascular endothelial damage. As previously reported, anti-endothelial cell antibodies (AECAs) are a heterogeneous group of autoantibodies against various cell surface proteins in endothelial cells and can contribute leucocyte adhesion by inducing adhesion molecules and cytokines in endothelial cells [34-36]. Anti-hnRNP-K antibody may thus be a class of AECA that becomes active under cold stimulation in patients with secondary RP. Further analyses are needed to elucidate the correlation of anti-hnRNP-K autoantibodies with the pathogenesis of secondary RP.

In summary, we provide the first evidence of cold-associated autoantibodies in patients with secondary RP. Anti-hnRNP-K antibody may be a potential biomarker for RP secondary to CTDs. Longitudinal studies are warranted to determine whether the evaluation of anti-hnRNP-K antibody in RP patients may aid in the detection of CTDs in these patients.

Rheumatology key messages

- Cold-associated autoantibody in patients with secondary RP is successfully identified by a proteomic approach.
- hn-RNP-K translocates to the endothelial cell surface upon cold stimulation.
- Anti-hnRNP-K autoantibody may serve as a biomarker for secondary RP.

Acknowledgements

Supplementary data

Supplementary data are available at *Rheumatology* Online.

References

1 Unwin RD, Griffiths JR, Whetton AD. Simultaneous analysis of relative protein expression levels across multiple samples using iTRAQ isobaric tags with 2D nano LC-MS/MS. Nat Protoc 2010;5:1574-82.

2 Serada S, Fujimoto M, Ogata A et al. iTRAQ-based proteomic identification of leucine-rich alpha-2 glycoprotein as a novel inflammatory biomarker in autoimmune diseases. Ann Rheum Dis 2010;69:770-4.

3 Yokoyama T, Enomoto T, Serada S et al. Plasma membrane proteomics identifies bone marrow stromal antigen 2 as a potential therapeutic target in endometrial cancer. Int J Cancer 2013;132:472-84.

4 Herrick AL. The pathogenesis, diagnosis and treatment of Raynaud phenomenon. Nat Rev Rheumatol 2012;8: 469-79.

5 Bakst R, Merola JF, Franks AG Jr, Sanchez M. Raynaud's phenomenon: pathogenesis and management. J Am Acad Dermatol 2008;59:633-53.

6 Dimant J, Ginzler E, Schlesinger M et al. The clinical significance of Raynaud's phenomenon in systemic lupus erythematosus. Arthritis Rheum 1979;22:815-9.

7 Grader-Beck T, Wigley FM. Raynaud's phenomenon in mixed connective tissue disease. Rheum Dis Clin North Am 2005;31:465-81, vi.

8 Maricq HR, Harper FE, Khan MM, Tan EM, LeRoy EC. Microvascular abnormalities as possible predictors of disease subsets in Raynaud phenomenon and early connective tissue disease. Clin Exp Rheumatol 1983;1: 195-205.

9 Srivastava R, Aslam M, Kalluri SR et al. Potassium channel KIR4.1 as an immune target in multiple sclerosis. N Engl J Med 2012;367:115-23.

10 Serada S, Fujimoto M, Takahashi T et al. Proteomic analysis of autoantigens associated with systemic lupus erythematosus: anti-aldolase A antibody as a potential marker of lupus nephritis. Proteomics Clin Appl 2007;1: 185-91.

11 He P, Naka T, Serada S et al. Proteomics-based identification of alpha-enolase as a tumor antigen in non-small lung cancer. Cancer Sci 2007;98:1234-40.

12 Masi AT. Preliminary criteria for the classification of systemic sclerosis (scleroderma). Subcommittee for scleroderma criteria of the American Rheumatism Association Diagnostic and Therapeutic Criteria Committee. Arthritis Rheum 1980;23:581-90.

13 Tan EM, Cohen AS, Fries JF et al. The 1982 revised criteria for the classification of systemic lupus erythematosus. Arthritis Rheum 1982;25:1271-7.

14 Hochberg MC. Updating the American College of Rheumatology revised criteria for the classification of systemic lupus erythematosus. Arthritis Rheum 1997;40: 1725.

15 Kasukawa R, Tojo T, Miyawaki S. Preliminary diagnostic criteria for classification of mixed connective tissue disease. In: Kasukawa R, Sharp GC, eds. Mixed Connective Tissue Diseases and Antinuclear Antibodies. Amsterdam, the Netherlands: Elsevier, 1987:41-7.

16 Brennan P, Silman A, Black C et al. Validity and reliability of three methods used in the diagnosis of Raynaud's phenomenon. The UK Scleroderma Study Group. Br J Rheumatol 1993;32:357-61.

17 Umegaki-Arao N, Tamai K, Nimura K et al. Karyopherin alpha2 is essential for rRNA transcription and protein synthesis in proliferative keratinocytes. PLoS One 2013;8: e76416.

18 Yang L, Serada S, Fujimoto M et al. Periostin facilitates skin sclerosis via PI3K/Akt dependent mechanism in a mouse model of scleroderma. PLoS One 2012;7: e41994.

19 Han SP, Tang YH, Smith R. Functional diversity of the hnRNPs: past, present and perspectives. Biochem J 2010; 430:379-92.

20 Dreyfuss G, Matunis MJ, Pinol-Roma S, Burd CG. hnRNP proteins and the biogenesis of mRNA. Annu Rev Biochem 1993;62:289-321.

21 Furukawa F, Kashihara-Sawami M, Lyons MB, Norris DA. Binding of antibodies to the extractable nuclear antigens SS-A/Ro and SS-B/La is induced on the surface of human keratinocytes by ultraviolet light (UVL): implications for the pathogenesis of photosensitive cutaneous lupus. J Invest Dermatol 1990;94:77-85.

22 Wang B, Dong X, Yuan Z, Zuo Y, Wang J. SSA/Ro antigen expressed on membrane of UVB-induced apoptotic keratinocytes is pathogenic but not detectable in supernatant of cell culture. Chin Med J 1999;112:512-5.

23 Golan TD, Elkon KB, Gharavi AE, Krueger JG. Enhanced membrane binding of autoantibodies to cultured keratinocytes of systemic lupus erythematosus patients after ultraviolet B/ultraviolet A irradiation. J Clin Invest 1992;90: 1067-76.

24 Nickel W, Seedorf M. Unconventional mechanisms of protein transport to the cell surface of eukaryotic cells. Annu Rev Cell Dev Biol 2008;24:287-308.

25 Nickel W, Rabouille C. Mechanisms of regulated unconventional protein secretion. Nat Rev Mol Cell Biol 2009;10: 148-55.

26 Nickel W. Pathways of unconventional protein secretion. Curr Opin Biotechnol 2010;21:621-6.

27 Bomsztyk K, Denisenko O, Ostrowski J. hnRNP K: one protein multiple processes. Bioessays 2004;26: 629-38.

28 Qi Z, Takamatsu H, Espinoza JL et al. Autoantibodies specific to hnRNP K: a new diagnostic marker for immune pathophysiology in aplastic anemia. Ann Hematol 2010; 89:1255-63.

29 Van den Bergh K, Hooijkaas H, Blockmans D et al. Heterogeneous nuclear ribonucleoprotein h1, a novel nuclear autoantigen. Clin Chem 2009;55:946-54.

30 Op De Beeck K, Maes L, Van den Bergh K et al. Heterogeneous nuclear RNPs as targets of autoantibodies in systemic rheumatic diseases. Arthritis Rheum 2012;64: 213-21.

31 D.S.G. Tobacco report: PHS Study Group, after 14-month survey, agrees that smoking is indeed harmful. Science 1964;143:227.

32 Buchanan RR, Riglar AG. The titre of anti-centromere antibodies: its relationship to Raynaud's phenomenon and vascular occlusion. Br J Rheumatol 1989;28:221–6.

33 Furtado RN, Pucinelli ML, Cristo VV, Andrade LE, Sato EI. Scleroderma-like nailfold capillaroscopic abnormalities are associated with anti-U1-RNP antibodies and Raynaud's phenomenon in SLE patients. Lupus 2002;11: 35–41.

34 Carvalho D, Savage CO, Black CM, Pearson JD. IgG antiendothelial cell autoantibodies from scleroderma patients induce leukocyte adhesion to human vascular endothelial cells in vitro. Induction of adhesion molecule expression and involvement of endothelium-derived cytokines. J Clin Invest 1996;97:111–9.

35 Del Papa N, Guidali L, Sironi M et al. Anti-endothelial cell IgG antibodies from patients with Wegener's granulomatosis bind to human endothelial cells in vitro and induce adhesion molecule expression and cytokine secretion. Arthritis Rheum 1996;39:758–66.

36 Lin CF, Chiu SC, Hsiao YL et al. Expression of cytokine, chemokine, and adhesion molecules during endothelial cell activation induced by antibodies against dengue virus nonstructural protein 1. J Immunol 2005;174:395–403.

Human herpesvirus 6 gM/gN complex interacts with v-SNARE in infected cells

Akiko Kawabata,[1] Satoshi Serada,[2] Tetsuji Naka[2] and Yasuko Mori[1]

Correspondence
Yasuko Mori
ymori@med.kobe-u.ac.jp

[1]Division of Clinical Virology, Center for Infectious Diseases, Kobe University Graduate School of Medicine, 7-5-1, Kusunoki-cho, Chuo-ku, Kobe 650-0017, Japan

[2]Laboratory of Immune Signal, Division of Biomedical Research, National Institute of Biomedical Innovation, 7-6-8, Saito-Asagi, Ibaraki, Osaka 567-0085, Japan

Human herpesvirus 6 (HHV-6) glycoprotein M (gM) is an envelope glycoprotein that associates with glycoprotein N (gN), forming the gM/gN protein complex, in a similar manner to the other herpesviruses. Liquid chromatography-MS/MS analysis showed that the HHV-6 gM/gN complex interacts with the v-SNARE protein, vesicle-associated membrane protein 3 (VAMP3). VAMP3 colocalized with the gM/gN complex at the *trans*-Golgi network and other compartments, possibly the late endosome in HHV-6-infected cells, and its expression gradually increased during the late phase of virus infection. Finally, VAMP3 was incorporated into mature virions and may be transported with the gM/gN complex.

INTRODUCTION

Human herpesvirus 6 (HHV-6) belongs to the betaherpesvirus subfamily (Roizmann *et al.*, 1992). HHV-6 isolates can be classified as HHV-6A and HHV-6B (Ablashi *et al.*, 2013) based on genetic and antigenic differences, cell tropism, and pathogenesis (Ablashi *et al.*, 1991; Aubin *et al.*, 1991; Campadelli-Fiume *et al.*, 1993; Chandran *et al.*, 1992; Mori, 2009; Yamanishi *et al.*, 1988).

Herpesviruses encode several glycoproteins on the envelope of viral particles that work for entry, assembly and egress of the virus. Of these, glycoprotein M (gM) is a remarkable envelope glycoprotein as it is conserved among all herpesvirus subfamilies. Most herpesviruses, including herpes simplex virus type-1 (Baines & Roizman, 1991), pseudorabies virus (Dijkstra *et al.*, 1996) and equine herpesvirus 1 (Osterrieder *et al.*, 1996), do not require gM for replication. Marek's disease virus (Tischer *et al.*, 2002) and varicella-zoster virus (Yamagishi *et al.*, 2008) abolish virus growth *in vitro*. However, the gM protein of human cytomegalovirus (HCMV), which belongs to the betaherpesvirus subfamily, is essential for the production of infectious virus (Hobom *et al.*, 2000).

HHV-6 gM is a product of the U72 ORF and comprises 343 aa (Kawabata *et al.*, 2012; Lawrence *et al.*, 1995). Post-infection (p.i.), it is translated into a 47–63 kDa protein that is post-translationally glycosylated (Kawabata *et al.*, 2012). It is a type III transmembrane protein with seven membrane-spanning domains and a C-terminal cytoplasmic tail. HHV-6 gM interacts with the product of the U46 ORF, known as gN, to form a complex for transport to the *trans*-Golgi network (TGN) and endosomal compartments (Kawabata *et al.*, 2012). Finally, the gM/gN complex is

incorporated into mature virions. Interestingly, unlike in alpha herpesviruses, HHV-6 gM is essential for virus growth (Kawabata *et al.*, 2012).

To further examine the role of HHV-6A gM during HHV-6 infection, we performed liquid chromatography (LC)-MS/MS analysis to identify the cellular components that interact with the gM/gN complex. The results showed that the gM/gN complex interacts with VAMP3 (vesicle-associated membrane protein 3).

VAMP3 is a v-SNARE (soluble *N*-ethylmaleimide-sensitive factor attachment protein receptor) protein that resides in recycling endosomes and endosome-derived transport vesicles. v-SNARE interacts with SNARE proteins on target membranes (t-SNAREs) to form *trans*-SNARE complexes, which draw the two membranes together and drive membrane fusion (Jahn & Scheller, 2006; Jahn *et al.*, 2003; Rothman, 1994; Söllner *et al.*, 1993). SNAREs are cytoplasmic-oriented type I membrane proteins that play a role in intracellular trafficking mechanisms during exocytosis by forming a complex that facilitates the transient fusion of the vesicular and plasma membrane lipid bilayers (Mohrmann & Sørensen, 2012). This membrane fusion is dependent on the formation of a complex between t-SNARE and v-SNARE proteins (Jahn & Scheller, 2006; Jahn *et al.*, 2003).

VAMP3 is localized to recycling endosomes (McMahon *et al.*, 1993) and plays a role in the fusion of recycling endosomes and the plasma membrane by forming a complex with the surface t-SNARE complex, Stx4/SNAP23 (Hu *et al.*, 2007). The VAMP3/Stx4/SNAP23 SNARE complex mediates the long-loop recycling pathway that delivers recycling endosomes and their cargo to the cell

surface, and plays an important role in regulating the ability of macrophages to effectively adhere and spread on fibronectin (Veale et al., 2011). VAMP3 is also involved in integrin trafficking, cell migration and cell adhesion (Luftman et al., 2009; Tayeb et al., 2005). In addition, it plays a role in the exocytosis of α-granules in platelets (Polgár et al., 2002), as well as in the recycling of endocytosed transferrin receptors to the cell surface (Galli et al., 1994).

Here, we describe the interaction between the gM/gN complex and VAMP3 in HHV-6A-infected cells and discuss the potential for the association between the gM/gN complex and VAMP3 to modify its localization and mediate its incorporation into mature virions.

RESULTS

Identification of cellular proteins interacting with the gM/gN complex

A recent study showed that the cytoplasmic tail of HCMV gM interacts with the cellular protein FIP4, which is a Rab11-GTPase effector protein important for gM/gN trafficking and for accumulation of the envelope glycoprotein complex in the assembly compartment in HCMV-infected cells (Krzyzaniak et al., 2009). To examine the function of HHV-6A gM/gN, we tried to identify the cellular protein(s) that interact with the gM/gN complex. First, gM and gN were cotransfected into 293T cells and gM was immunoprecipitated from the lysates with an anti-gM mAb. Silver staining of gels containing proteins separated from the lysates of the gM/gN-expressing cells revealed several specific bands at approximately 10 kDa; these proteins were not present in the lysates of cells expressing gM alone. One specific band (Fig. 1a, arrowhead) was excised from the gel and subjected to LC-MS/MS analysis. The results of this analysis identified VAMP3 as the interacting protein (Fig. 1b).

To confirm the interaction between VAMP3 and gM/gN, lysates from cells expressing both HA-tagged gM and FLAG-tagged gN were immunoprecipitated with an anti-HA antibody, followed by Western blotting with anti-gM, anti-FLAG or anti-VAMP3 antibodies. As shown in Fig. 1c, VAMP3 was coprecipitated when gM and gN were coexpressed. However, VAMP3 was not coprecipitated when gM or gN was expressed alone. CD63 was not coprecipitated even when gM and gN were coexpressed (Fig. 1c). These results indicate that VAMP3 interacts with the gM/gN complex.

Interaction between gM and VAMP3 in HHV-6A-infected cells

To confirm the interaction between the gM/gN complex and VAMP3 in HHV-6A-infected cells, lysates from HHV-6A-infected HSB-2 cells were immunoprecipitated with an anti-gM mAb or an anti-VAMP3 antibody, followed by Western blotting with anti-gM, anti-VAMP3, anti-CD63 or

anti-gB antibodies (Fig. 2). Endogenous VAMP3 coprecipitated with gM and vice versa; gB or endogenous CD63 coprecipitated with neither gM nor VAMP3 (Fig. 2b). These results indicate that gM also interacts with VAMP3 in HHV-6A-infected cells. Interestingly, although gM with a molecular mass of 15 kDa was detected in the lysates of HHV-6A-infected cells, it did not coprecipitate with the anti-VAMP3 antibody.

To examine the cellular localization of gM and VAMP3 in HHV-6A-infected cells, an indirect immunofluorescence assay (IFA) was performed using HHV-6A-infected HSB-2 cells at 96 h p.i. (Fig. 3). Confocal microscopy of HHV-6A-infected HSB-2 cells showed that gM and VAMP3 appear to partially colocalize to the same cellular compartment. In addition, gM and VAMP3 partially colocalized with TGN46, a marker of the TGN (Fig. 3b), and with CD63, a marker of late endosomes and multivesicular bodies (MVB) (Fig. 3a). The expression of endogenous VAMP3 was much lower in uninfected cells than infected cells [Fig. 3a(ii), b(ii)]. These results indicate that VAMP3 may localize with gM to the endosomal compartment in addition to TGN during the late stage of infection. Preimmune serum of guinea pig did not react with either HHV-6A-infected [Fig. 3d(i)] or uninfected cells [Fig. 3d(ii)], although anti-VAMP3 antibody obtained from the same guinea pig reacted with HHV-6A-infected cells [Fig. 3c(i)] but not uninfected cells [Fig. 3c(ii)].

VAMP3 is present in purified HHV-6A virions

Recently, we showed that HHV-6A virions are released through MVBs via the cellular exosomal pathway and that gB and gM are present on exosomes (Mori et al., 2008). To examine whether VAMP3 expressed in HHV-6A-infected cells is present on virions and exosomes, we purified virions from the culture medium of HHV-6A-infected cells. As expected, VAMP3, gM and CD63 were detected by western blotting of the virion fractions (Fig. 4a). Virion fractions were confirmed with the presence of gB (Fig. 4a) and viral DNA (Fig. 4b). In addition, VAMP3 was detected on HHV-6A virions by immunogold labelling electron microscopy analysis [Fig. 4c(i)], but it was rarely detected on virions without primary antibody [Fig. 4c(ii)]. These results indicate that VAMP3 is incorporated into viral particles along with the gM/gN complex.

### Intracellular localization of the gM/gN complex and VAMP3 in cells transiently expressing gM/gN

We next examined the intracellular localization of gM, gN and VAMP3 (Fig. 5). When plasmids expressing gM and gN were cotransfected into HeLa cells [Fig. 5a(i)], gM/gN colocalized with endogenous VAMP3 in the perinuclear region. However, when gM was expressed alone, it failed to colocalize with VAMP3 [Fig. 5a(ii)]. Because the gM/gN complex localized to the TGN in HHV-6A-infected cells, we hypothesized that the gM/gN complex would interact with
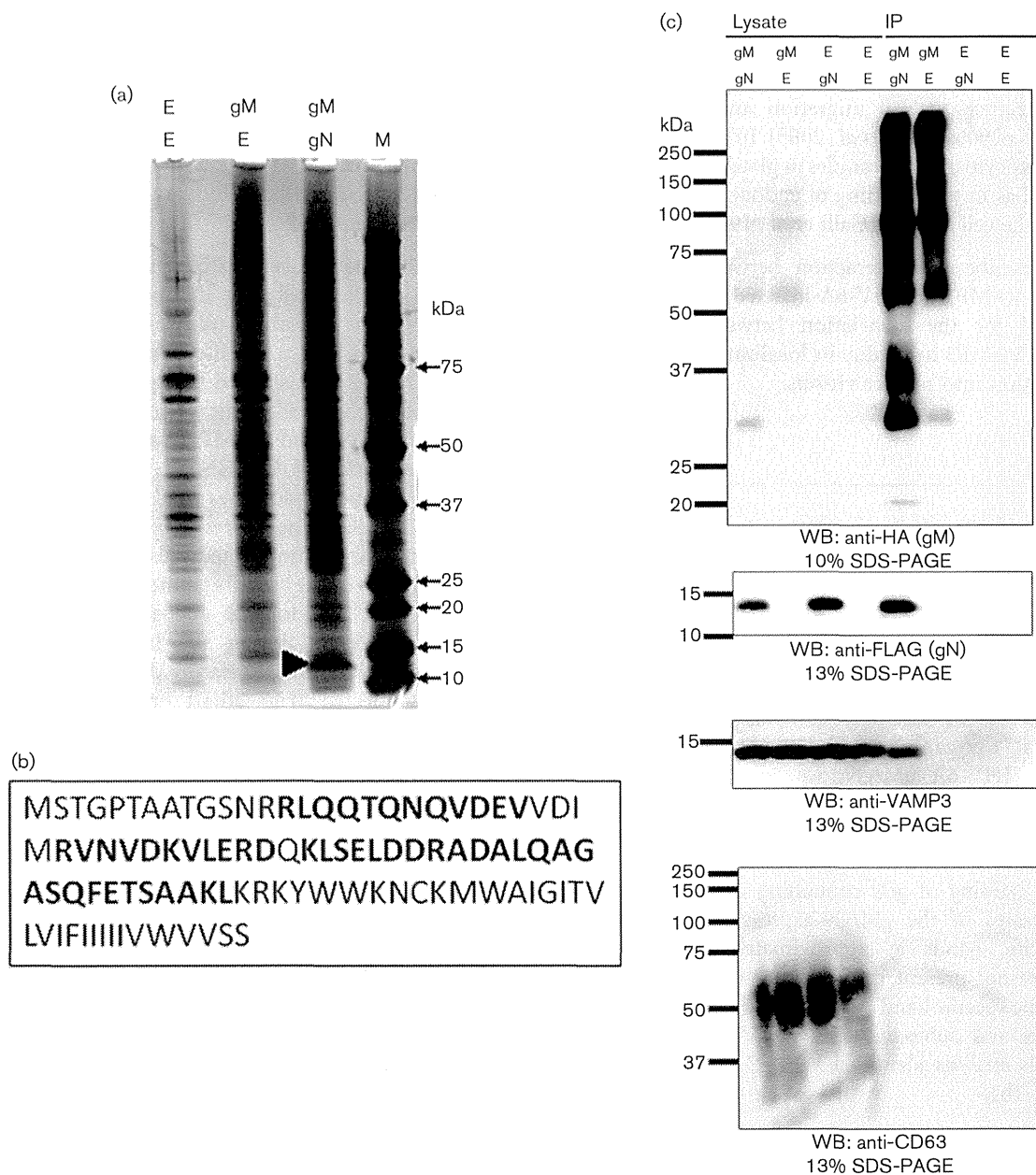
Fig. 1. Interaction between gM/gN and VAMP3. (a) 293T cells were transfected with plasmids expressing HA-tagged gM and FLAG-tagged gN. The cells were lysed with TNE buffer at 72 h post-transfection. The lysates were then immunoprecipitated with an anti-HA Ab specific for gM and visualized by silver staining. The band marked by the arrowhead indicates the protein selected for analysis by LC-MS/MS. (b) Peptide matches to the VAMP3 sequence are shown in bold. (c) 293T cells were transfected with plasmids expressing HA-tagged gM, FLAG-tagged gN, or pCAGGS (negative control). The cells were then lysed with TNE buffer at 72 h post-transfection. The lysates were immunoprecipitated with anti-HA antibody for gM and analysed by Western blotting with anti-HA, anti-FLAG, anti-VAMP3 (BioReagents) or anti-CD63 antibodies. The numbers beside the panels indicate the molecular masses (kDa). WB, Western blotting; E, empty.

VAMP3 at the TGN or a TGN-derived compartment. As expected, when gM was coexpressed with gN, it colocalized with VAMP3 and TGN46 (Fig. 5b); however, this colocalization was not observed when gM was expressed alone [Fig. 5a(ii)]. These results suggest that the interaction between the gM/gN complex and VAMP3 occurs at the TGN or a TGN-derived compartment. Glycoprotein M did not colocalize with CD63 even when gM was coexpressed with gN [Fig. 4c(i)]. Non-specific staining of gM was not seen in these cells [Fig. 5a(iii), b(ii), c(ii)].
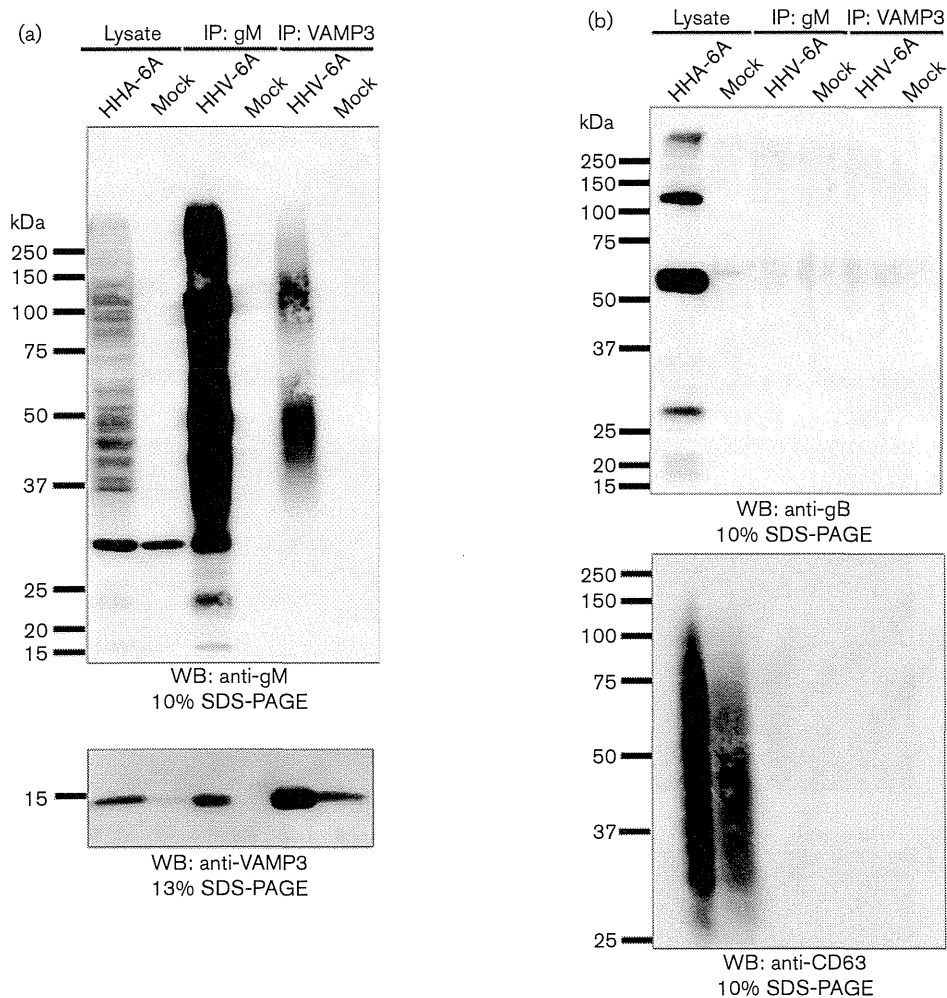
Fig. 2. Interaction between gM and VAMP3 in HHV-6A-infected HSB-2 cells. HHV-6A-infected or mock-infected HSB-2 cells were lysed with TNE buffer at 96 h post-infection. The lysates were immunoprecipitated (IP) with anti-gM mAb or anti-VAMP3 Ab (see Methods) and analysed by Western blotting with anti-gM or anti-VAMP3 (BioReagents) Abs (a), anti-gB Ab or anti-CD63 mAb (b). The numbers beside the panels indicate the molecular masses (kDa). WB, Western blotting.

## The kinetics of VAMP3 expression in HHV-6A-infected cells

As shown in Fig. 2, VAMP3 expression in HHV-6A-infected cells was higher than that in mock-infected cells. Therefore, we examined the kinetics of VAMP3 expression in HHV-6A-infected cells. The results in Fig. 6 show that VAMP3 expression increased gradually in the infected cells.

DISCUSSION

Here, we used the transient expression of gM and gN to identify VAMP3 as a cellular molecule that interacts with the HHV-6A gM/gN complex. The interaction between VAMP3 and the gM/gN complex was also confirmed in HHV-6A-infected cells. VAMP3 and gM/gN proteins colocalized at the TGN in cells coexpressing gM and gN, and

in HHV-6A-infected cells. This interaction was observed only when gM/gN formed a complex, indicating that the interaction is required for gM/gN complex formation. Previously, we reported that the localization of HHV-6A gM to the TGN was necessary for its interaction with gN (Kawabata *et al.*, 2012). Therefore, the interaction between the gM/gN complex and VAMP3 might also occur at the TGN. It is still not known whether the interaction between VAMP3 and gM requires gM/gN complex formation. Transport of gM to the TGN might be required for this interaction.

VAMP3 also colocalized with CD63, which is a marker of late endosome in HHV-6A-infected cells. In cells transiently expressing gM and gN, however, VAMP3 colocalized with TGN46, but not CD63. This suggests that in infected cells, the localization of VAMP3 may be modified through its interaction with gM/gN, thereby possibly allowing it to localize to the other organelles, such as the late endosome.
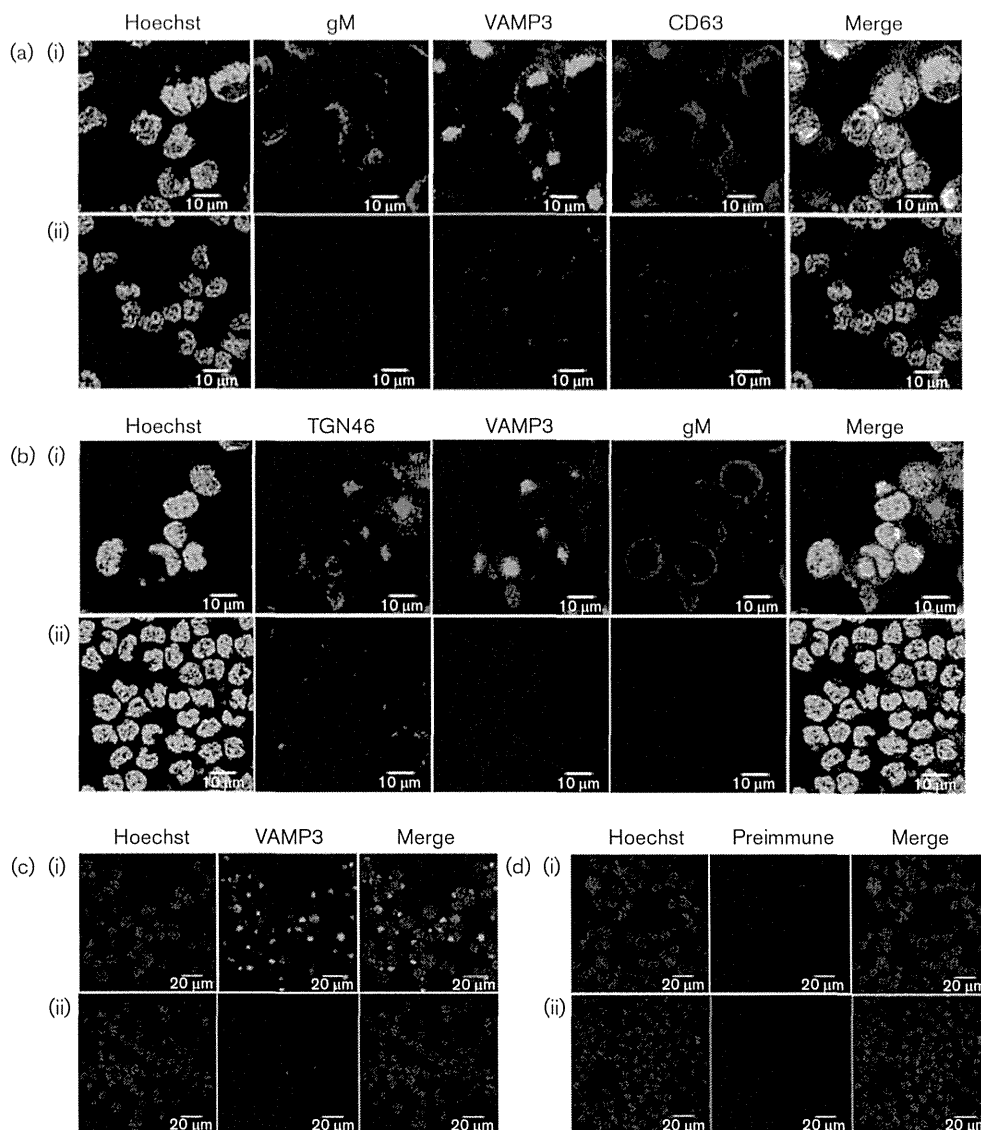
Fig. 3. Colocalization of gM, VAMP3 and CD63, or gM, VAMP3 and TGN46 in HHV-6A-infected cells. HHV-6A-infected [a(i), b(i)] or mock-infected [a(ii), b(ii)] HSB-2 cells were harvested at 96 h post-infection and fixed. The cells were stained with antibodies against VAMP3, gM and CD63 as well as with Hoechst 33258 (a), or VAMP3, gM and TGN46 as well as with Hoechst 33258 (b). Costained areas appear white in the merged panel. Bars, 10 μm. HHV-6A-infected [c(i), d(i)] or mock-infected [c(ii), d(ii)] cells were stained with guinea pig antisera against VAMP3 (c) or preimmune sera obtained from the same guinea pig as well as with Hoechst 33258 (d). Bars, 20 μm.

We also found that VAMP3 was incorporated into virions. As the gM/gN complex is expressed on virions and exosomes, complex-associated VAMP3 would be transported along with the gM/gN complex and then released via the exosomal release pathway (Mori *et al.*, 2008).

Although the function of VAMP3 in HHV-6A-infected cells is not known, its interaction with the gM/gN complex may modify the cellular machinery in infected cells. As VAMP3 is incorporated into virions and exosomes, its primary function (to facilitate membrane fusion) may be lost in infected cells. Overexpression of VAMP3 did not

affect HHV-6 growth (data not shown). Several v-SNARE proteins with functions similar to those of VAMP3 have been identified (Borisovska *et al.*, 2005). Therefore, the function of VAMP3 may be redundant in HHV-6A-infected cells. It is still not known whether v-SNAREs, including VAMP3, are required for HHV-6 infection. Further studies will be required to address these questions.

METHODS

Cells and viruses. The HSB-2 T-cell line was cultured in RPMI 1640 medium (Nissui) supplemented with 8 % FBS. Human embryonic
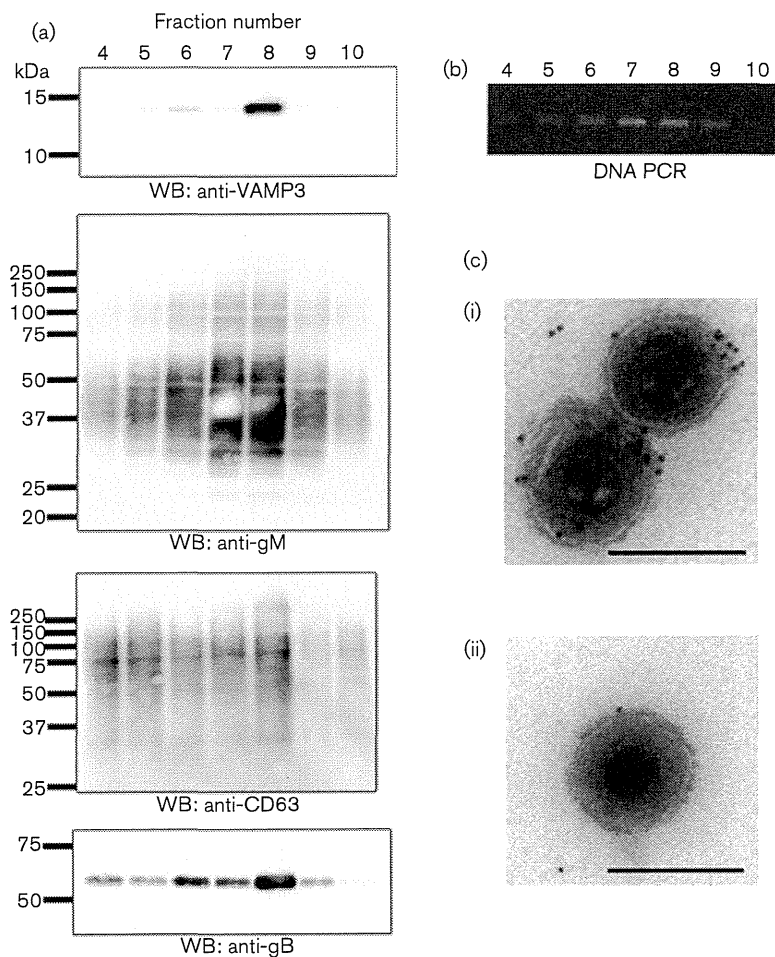
Fig. 4. The presence of VAMP3 in HHV-6A virions and exosomes. Exosome fractions containing virions were purified from the culture medium of HHV-6A-infected cells by sucrose density-gradient centrifugation and then analysed by Western blotting (a), DNA PCR (b) and electron microscopy (c). (a) Western blot analysis of the sucrose density-gradient fractions with anti-VAMP3, anti-gM, anti-CD63 or anti-gB Abs. (b) Viral DNA was detected in the fractions by PCR with HHV-6A specific primers. The numbers above the PCR image showed the fraction numbers. (c) Immunogold localization of VAMP3 on the HHV-6A virions. Purified virions (fraction 8) were labelled with antisera against VAMP3 (i) or without primary antibody (ii). Bars, 200 nm.

kidney cells (293T cells) and HeLa cells were cultured in Dulbecco's modified Eagle's medium supplemented with 8 % FBS. The HHV-6A strain GS was propagated and titrated in HSB-2 cells. HHV-6A cell-free virus was prepared as previously described (Akkapaiboon et al., 2004). Cord blood mononuclear cells (CBMC) were used for virus propagation (Mori et al., 2004). CBMCs were kindly provided by K. Adachi (Minoh Hospital, Minoh, Japan) and H. Yamada (Kobe University Graduate School of Medicine, Kobe, Japan) and purchased from the RIKEN Cell Bank (BioResource Center). For the usage of CBMCs, the study was approved by the ethics committee of each institution.

Antibodies. Rabbit antibody (Ab) specific for HHV-6A gM or gB (Mori et al., 2008), an AgM-1 mAb against gM (Kawabata et al., 2012), and a U14 mAb against HHV-6 U14 (Takemoto et al., 2005) were used. mAbs against CD63 (clone CLB-gran/12, 435; Sanquin) and α-tubulin (clone B-5-1-2; Sigma), a sheep polyclonal Ab against TGN46 (AbD Serotec), a rabbit polyclonal Ab against VAMP3 (BioReagents) and a goat polyclonal Ab against VAMP3 (Santa Cruz) were used. Anti-HA (clone HA-7; Sigma) and anti-FLAG (clone M2; Sigma) antibodies were also used. Alexa Fluor 594-conjugated donkey anti-sheep IgG (Molecular Probes), Alexa Fluor 594-conjugated donkey anti-rabbit IgG (Molecular Probes), FITC-conjugated affinity pure F(ab')₂ fragment goat anti-guinea pig IgG (Jackson ImmunoResearch Laboratories), and Cy5-conjugated donkey anti-mouse IgG (Jackson ImmunoResearch Laboratories) were used as secondary antibodies. An anti-VAMP3 monospecific Ab was produced by subjecting guinea pigs to three rounds of immunization with the antigen, which was then expressed in Escherichia coli and purified (Mori et al., 2008).

Immunofluorescence assay. The IFA was performed as described previously (Akkapaiboon et al., 2004; Mori et al., 2004). Specific immunofluorescence was observed under a confocal laser-scanning microscope (FluoView FV1000; Olympus).

Plasmid construction. The HA-tagged gM- and FLAG-tagged gN-expressing plasmids were described previously (Kawabata et al., 2012). The pCAGGS plasmid was kindly provided by Jun-ichi Miyazaki (Osaka University, Japan) (Niwa et al., 1991). To express the recombinant protein, the following primer pair was used to amplify inserts from HSB-2 cells cDNA: for named GST-VAMP3, VAMP3FbamHI (5'-ACCGGATCCTCTACAGGTCCAACTGCTGC-CACT-3') and VAMP3rsalI (5'-ACCGTCGACTTACTTGCAATTCT-TCCACCAATATTTC-3'). The PCR products were inserted into the pGEX-4T1 vector (GE Healthcare).

Plasmid transfection. HeLa cells were transfected with the expression plasmids using Lipofectamine 2000 (Invitrogen) according to the manufacturer's instructions. The 293T cells were transfected using the calcium phosphate method as described previously (Koshizuka et al., 2010).

Identification of gM/gN-interacting proteins. Plasmids expressing HA-tagged gM and FLAG-tagged gN were cotransfected into 293T cells. Cotransfection of gM and pCAGGS into 293T cells was performed as a control. At 72 h post-transfection, the cells were lysed in TNE buffer (0.01 M Tris/HCl, pH 7.4, 0.15 M NaCl, 1 mM EDTA, 1 % Nonidet-P-40). After centrifugation at 200 000 g for 1 h, the
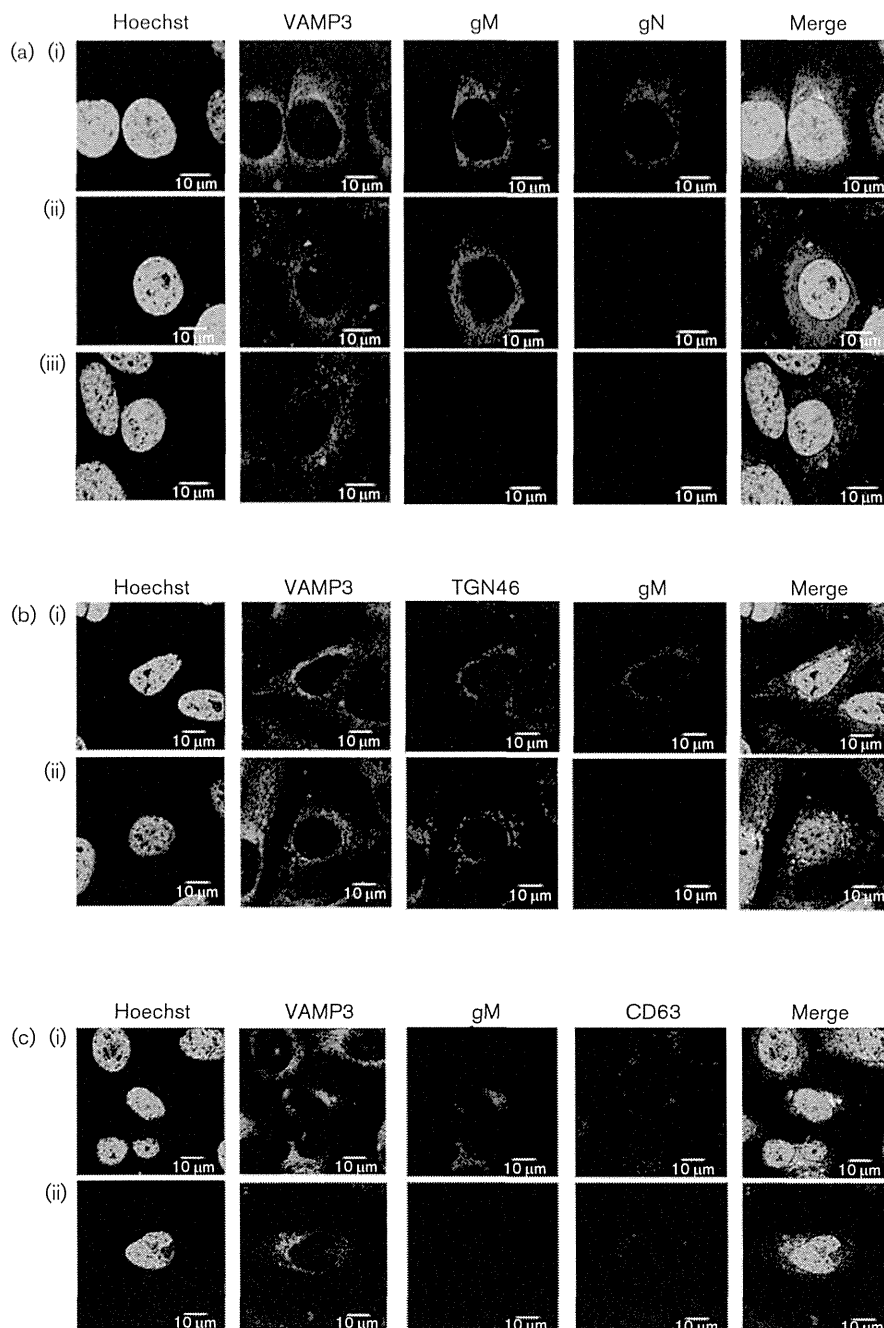
Fig. 5. Subcellular localization of VAMP3 with the gM/gN complex in HeLa cells transiently expressing gM and gN. HeLa cells were transfected with plasmids expressing gM and gN [a(i), b(i), c(i)], gM and the empty vector [a(ii)], or without vectors [a(iii), b(ii), c(ii)]. The cells were harvested at 48 h post-transfection and fixed. (a) The cells were stained with antibodies against gM, FLAG (for gN) and VAMP3 as well as with Hoechst 33258. (b) Cells were stained with antibodies against gM, TGN46 and VAMP3 as well as Hoechst 33258. (c) Cells were stained with antibodies against gM, CD63 and VAMP3 as well as with Hoechst 33258. Co-stained areas appear white or yellow in the merged panel. Bars, 10 μm.

supernatants were incubated overnight at 4 °C with an anti-HA antibody conjugated to protein G Sepharose (GE Healthcare). The protein-anti-HA conjugated beads were then washed with lysis buffer and the bound proteins were eluted with 0.1 M glycine/HCl (pH 2.8). After the beads were removed by centrifugation, the supernatants were

neutralized by adding 1 M Tris-HCl (pH 9.5). The eluted proteins were then solubilized with sample buffer, separated on a NuPAGE SDS-PAGE system (Invitrogen), and examined by silver staining. Specific bands were analysed by LC-MS/MS to identify the coimmunoprecipitated proteins (Shevchenko *et al.*, 1996; Tang *et al.*, 2013).
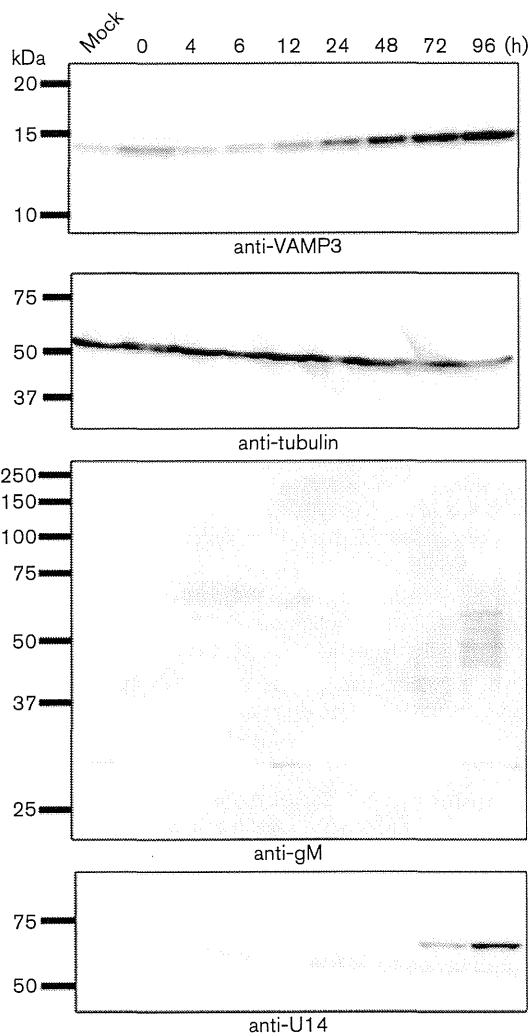
Fig. 6. Kinetics of VAMP3 protein expression in HHV-6A-infected cells. Whole-cell lysates collected at the indicated time points (h) were analysed by Western blotting. The numbers beside the panels indicate the molecular masses (kDa).

Western blotting. Western blotting was performed as described previously (Akkapaiboon et al., 2004).

Isolation of virion fractions. Virions containing exosomes were collected from the cell culture medium by differential centrifugation and fractionated with a linear sucrose gradient, as described previously (Mori et al., 2008). The fractions were analysed by Western blotting, DNA PCR, and electron microscopy.

Electron microscopy. Immunogold labelling of virions was performed as described previously (Mori et al., 2008). The samples were examined under a Hitachi H-7650 electron microscope.

ACKNOWLEDGEMENTS

REFERENCES

Ablashi, D. V., Balachandran, N., Josephs, S. F., Hung, C. L., Krueger, G. R., Kramarsky, B., Salahuddin, S. Z. & Gallo, R. C. (1991). Genomic polymorphism, growth properties, and immunologic variations in human herpesvirus-6 isolates. *Virology* 184, 545–552.

Ablashi, D., Agut, H., Alvarez-Lafuente, R., Clark, D. A., Dewhurst, S., Diluca, D., Flamand, L., Frenkel, N., Gallo, R. & other authors (2014). Classification of HHV-6A and HHV-6B as distinct viruses. *Arch Virol* 159, 863–870.

Akkapaiboon, P., Mori, Y., Sadaoka, T., Yonemoto, S. & Yamanishi, K. (2004). Intracellular processing of human herpesvirus 6 glycoproteins Q1 and Q2 into tetrameric complexes expressed on the viral envelope. *J Virol* 78, 7969–7983.

Aubin, J. T., Collandre, H., Candotti, D., Ingrand, D., Rouzioux, C., Burgard, M., Richard, S., Huraux, J. M. & Agut, H. (1991). Several groups among human herpesvirus 6 strains can be distinguished by Southern blotting and polymerase chain reaction. *J Clin Microbiol* 29, 367–372.

Baines, J. D. & Roizman, B. (1991). The open reading frames UL3, UL4, UL10, and UL16 are dispensable for the replication of herpes simplex virus 1 in cell culture. *J Virol* 65, 938–944.

Borisovska, M., Zhao, Y., Tsytsyura, Y., Glyvuk, N., Takamori, S., Matti, U., Rettig, J., Südhof, T. & Bruns, D. (2005). v-SNAREs control exocytosis of vesicles from priming to fusion. *EMBO J* 24, 2114–2126.

Campadelli-Fiume, G., Guerrini, S., Xiaoming, L. & Foà-Tomasi, L. (1993). Monoclonal antibodies to glycoprotein B differentiate human herpesvirus 6 into two clusters, variants A and B. *J Gen Virol* 74, 2257–2262.

Chandran, B., Tirawatnapong, S., Pfeiffer, B. & Ablashi, D. V. (1992). Antigenic relationships among human herpesvirus-6 isolates. *J Med Virol* 37, 247–254.

Dijkstra, J. M., Visser, N., Mettenleiter, T. C. & Klupp, B. G. (1996). Identification and characterization of pseudorabies virus glycoprotein gM as a nonessential virion component. *J Virol* 70, 5684–5688.

Galli, T., Chilcote, T., Mundigl, O., Binz, T., Niemann, H. & De Camilli, P. (1994). Tetanus toxin-mediated cleavage of cellubrevin impairs exocytosis of transferrin receptor-containing vesicles in CHO cells. *J Cell Biol* 125, 1015–1024.

Hobom, U., Brune, W., Messerle, M., Hahn, G. & Koszinowski, U. H. (2000). Fast screening procedures for random transposon libraries of cloned herpesvirus genomes: mutational analysis of human cytomegalovirus envelope glycoprotein genes. *J Virol* 74, 7720–7729.

Hu, C., Hardee, D. & Minnear, F. (2007). Membrane fusion by VAMP3 and plasma membrane t-SNAREs. *Exp Cell Res* 313, 3198–3209.

Jahn, R. & Scheller, R. H. (2006). SNAREs–engines for membrane fusion. *Nat Rev Mol Cell Biol* 7, 631–643.

Jahn, R., Lang, T. & Südhof, T. C. (2003). Membrane fusion. *Cell* 112, 519–533.

Kawabata, A., Jasirwan, C., Yamanishi, K. & Mori, Y. (2012). Human herpesvirus 6 glycoprotein M is essential for virus growth and requires glycoprotein N for its maturation. *Virology* 429, 21–28.

Koshizuka, T., Ota, M., Yamanishi, K. & Mori, Y. (2010). Characterization of varicella-zoster virus-encoded ORF0 gene–comparison of parental and vaccine strains. *Virology* 405, 280–288.

Krzyzaniak, M. A., Mach, M. & Britt, W. J. (2009). HCMV-encoded glycoprotein M (UL100) interacts with Rab11 effector protein FIP4. *Traffic* **10**, 1439–1457.

Lawrence, G. L., Nicholas, J. & Barrell, B. G. (1995). Human herpesvirus 6 (strain U1102) encodes homologues of the conserved herpesvirus glycoprotein gM and the alphaherpesvirus origin-binding protein. *J Gen Virol* **76**, 147–152.

Luftman, K., Hasan, N., Day, P., Hardee, D. & Hu, C. (2009). Silencing of VAMP3 inhibits cell migration and integrin-mediated adhesion. *Biochem Biophys Res Commun* **380**, 65–70.

McMahon, H. T., Ushkaryov, Y. A., Edelmann, L., Link, E., Binz, T., Niemann, H., Jahn, R. & Südhof, T. C. (1993). Cellubrevin is a ubiquitous tetanus-toxin substrate homologous to a putative synaptic vesicle fusion protein. *Nature* **364**, 346–349.

Mohrmann, R. & Sørensen, J. B. (2012). SNARE requirements en route to exocytosis: from many to few. *J Mol Neurosci* **48**, 387–394.

Mori, Y. (2009). Recent topics related to human herpesvirus 6 cell tropism. *Cell Microbiol* **11**, 1001–1006.

Mori, Y., Akkapaiboon, P., Yonemoto, S., Koike, M., Takemoto, M., Sadaoka, T., Sasamoto, Y., Konishi, S., Uchiyama, Y. & Yamanishi, K. (2004). Discovery of a second form of tripartite complex containing gH-gL of human herpesvirus 6 and observations on CD46. *J Virol* **78**, 4609–4616.

Mori, Y., Koike, M., Moriishi, E., Kawabata, A., Tang, H., Oyaizu, H., Uchiyama, Y. & Yamanishi, K. (2008). Human herpesvirus-6 induces MVB formation, and virus egress occurs by an exosomal release pathway. *Traffic* **9**, 1728–1742.

Niwa, H., Yamamura, K. & Miyazaki, J. (1991). Efficient selection for high-expression transfectants with a novel eukaryotic vector. *Gene* **108**, 193–199.

Osterrieder, N., Neubauer, A., Brandmuller, C., Braun, B., Kaaden, O. R. & Baines, J. D. (1996). The equine herpesvirus 1 glycoprotein gp21/22a, the herpes simplex virus type 1 gM homolog, is involved in virus penetration and cell-to-cell spread of virions. *J Virol* **70**, 4110–4115.

Polgár, J., Chung, S. H. & Reed, G. L. (2002). Vesicle-associated membrane protein 3 (VAMP-3) and VAMP-8 are present in human platelets and are required for granule secretion. *Blood* **100**, 1081–1083.

Roizmann, B., Desrosiers, R. C., Fleckenstein, B., Lopez, C., Minson, A. C., Studdert, M. J. & The Herpesvirus Study Group of the International Committee on Taxonomy of Viruses (1992). The family *Herpesviridae*: an update. *Arch Virol* **123**, 425–449.

Rothman, J. E. (1994). Mechanisms of intracellular protein transport. *Nature* **372**, 55–63.

Shevchenko, A., Wilm, M., Vorm, O. & Mann, M. (1996). Mass spectrometric sequencing of proteins silver-stained polyacrylamide gels. *Anal Chem* **68**, 850–858.

Söllner, T., Whiteheart, S. W., Brunner, M., Erdjument-Bromage, H., Geromanos, S., Tempst, P. & Rothman, J. E. (1993). SNAP receptors implicated in vesicle targeting and fusion. *Nature* **362**, 318–324.

Takemoto, M., Koike, M., Mori, Y., Yonemoto, S., Sasamoto, Y., Kondo, K., Uchiyama, Y. & Yamanishi, K. (2005). Human herpesvirus 6 open reading frame U14 protein and cellular p53 interact with each other and are contained in the virion. *J Virol* **79**, 13037–13046.

Tang, H., Serada, S., Kawabata, A., Ota, M., Hayashi, E., Naka, T., Yamanishi, K. & Mori, Y. (2013). CD134 is a cellular receptor specific for human herpesvirus-6B entry. *Proc Natl Acad Sci U S A* **110**, 9096–9099.

Tayeb, M. A., Skalski, M., Cha, M. C., Kean, M. J., Scaife, M. & Coppolino, M. G. (2005). Inhibition of SNARE-mediated membrane traffic impairs cell migration. *Exp Cell Res* **305**, 63–73.

Tischer, B. K., Schumacher, D., Messerle, M., Wagner, M. & Osterrieder, N. (2002). The products of the UL10 (gM) and the UL49.5 genes of Marek's disease virus serotype 1 are essential for virus growth in cultured cells. *J Gen Virol* **83**, 997–1003.

Veale, K. J., Offenhäuser, C., Lei, N., Stanley, A. C., Stow, J. L. & Murray, R. Z. (2011). VAMP3 regulates podosome organisation in macrophages and together with Stx4/SNAP23 mediates adhesion, cell spreading and persistent migration. *Exp Cell Res* **317**, 1817–1829.

Yamagishi, Y., Sadaoka, T., Yoshii, H., Somboonthum, P., Imazawa, T., Nagaike, K., Ozono, K., Yamanishi, K. & Mori, Y. (2008). Varicella-zoster virus glycoprotein M homolog is glycosylated, is expressed on the viral envelope, and functions in virus cell-to-cell spread. *J Virol* **82**, 795–804.

Yamanishi, K., Shiraki, K., Kondo, T., Okuno, T., Takahashi, M., Asano, Y. & Kurata, T. (1988). Identification of human herpesvirus-6 as a causal agent for exanthem subitum. *Lancet* **331**, 1065–1067.

– 408 –

Identification of Sialylated Glycoproteins in Doxorubicin-Treated Hepatoma Cells with Glycoproteomic Analyses

Kanako Azuma,[†] Satoshi Serada,[‡] Shinji Takamatsu,[†] Naoko Terao,[†] Shunsaku Takeishi,[§] Yoshihiro Kamada,[†] Tetsuji Naka,[‡] and Eiji Miyoshi*,[†]

[†]Department of Molecular Biochemistry & Clinical Investigation, Osaka University Graduate School of Medicine, Osaka 565-0871, Japan

[‡]Laboratory for Immune Signal, National Institute of Biomedical Innovation, Osaka 567-0085, Japan

[§]Department of Gastroenterology and Oncology, Institute of Health Biosciences, The University of Tokushima Graduate School, Tokushima 770-0855, Japan

ⓢ Supporting Information

ABSTRACT: Sialylation is one of the most important types of glycosylation involved in carcinogenesis and establishment of cancer stemness. We previously showed that increased sialylation is a characteristic glycan change in cancer stem cells (CSCs) from hepatocellular carcinoma. However, the identities of glycoproteins targeted for sialylation remain unknown. In the present study, we identified glycoproteins targeted for sialylation in doxorubicin (DXR)-treated hepatocarcinoma cell line, Huh7, using glycoproteomic analyses. Since CSCs constitute a small subset of cells within carcinoma cell lines, it is difficult to identify sialylated proteins using general glycoproteomic strategies. It is known that treatment with anticancer drug can condense CSCs, we used DXR to concentrate CSCs. In DXR-treated Huh7 cells, isobaric tag for relative and absolute quantitation (iTRAQ) analysis identified 17 sialylated glycoproteins. Most of the identified glycoproteins were cancer-associated proteins. Furthermore, two proteins of approximately 70 kDa were detected using Sambucus sieboldoana agglutinin (SSA) blot analysis and identified as beta-galactosidase and alpha-2-HS-glycoprotein (fetuin-A) by SSA precipitation followed by liquid chromatography-tandem mass spectrometry analyses. Sialylation levels of fetuin-A were increased in DXR-treated Huh7 cell lysates. These changes in sialylation of glycoproteins might be involved in the establishment of cancer stemness.

KEYWORDS: sialylation, cancer stem cells, doxorubicin, hepatoma, glycoproteomics
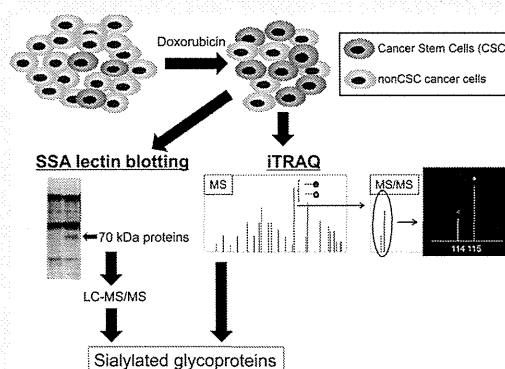
■ INTRODUCTION

A growing body of evidence suggests that tumors are frequently composed of heterogeneous cell types and that tumor initiation and growth are driven by a small subset of cells, termed cancer stem cells (CSCs), or tumor-initiating cells.[1−3] Several lines of research have indicated that CSCs can be preferentially resistant to many current therapies, including various chemotherapeutic agents and radiation treatment.[4−7] Thus, therapeutic strategies that effectively target CSCs could have a major impact on cancer patient survival. There are many reports on CSC markers, which include CD13,[8] CD44,[9,10] epithelial cell adhesion molecule (EpCAM),[11] and CD133.[9,12,13] These CSC markers have been used for identifying or concentrating CSCs in each type of cancer. It is unknown whether pure CSCs or whether heterogeneous populations containing CSC-like cells, should be targets for therapeutic strategies. Glycans are often attached to proteins and lipids on the cell surface and structurally and functionally modify these molecules. Glycans consist of several kinds of monosaccharides and show great structural diversity. Research in the field of glycobiology has revealed diverse and complex biological roles for these glycans.[14] The structures and amounts of glycans present on the cell surface change

dramatically during development and differentiation.[15] We have recently reported that sialylated glycans are useful markers for CSC-like cells in hepatoma cell lines.[16] Glycomic analysis using a lectin microarray showed marked binding of Sambucus sieboldoana agglutinin (SSA) to a CD133+CD13+ cell subpopulation within hepatoma cell lines. SSA lectin recognizes α2, 6-sialic acid.[16] Sialic acid is one of the building blocks of glycans and is generally found at the outermost ends of the glycan chains of glycoproteins and glycolipids. Thus, sialic acid is associated with many physiological and pathological events, including binding to infectious pathogens, regulation of immune responses, and tumor malignancy.[17] In particular, the alteration of sialic acid moieties is associated with cancer cell behavior, such as invasiveness and metastasis.[18−23] Glycan changes are involved in development and differentiation, and sialic acid is one of the most important glycosylations involved in these processes.[24]

In terms of glycoproteomic analyses, the identification of target proteins for each characteristic oligosaccharide structure is very important.[25] However, using the conventional strategy, which involves pooling and concentrating the CSC fraction using CD markers and lectins, it was not easy to obtain appropriate amounts of proteins for glycomic analyses. In general, CSC or CSC-like cells are resistant to anticancer drug treatment. For example, a CD133 and SSA double-positive population was resistant to several kinds of anticancer drug treatments such as 5-fluorouracil (5-FU) (Supplementary Figure 1). Hermann et al. also showed that the number of CD133-positive cells increased in human pancreatic cancer cells treated with gemcitabine.[26] These results suggest that short-term treatment with anticancer drugs can be used to easily concentrate CSCs. Among emerging proteomic technologies, isobaric tags for relative and absolute quantitation (iTRAQ) is a shotgun-based technique, which allows the concurrent identification and relative quantification of hundreds of proteins from different biological samples in a single experiment.[27,28] Whereas iTRAQ analysis leads to a more comprehensive analysis of sialylated proteins, the SSA lectin precipitation technique followed by liquid chromatography– tandem mass spectrometry (LC–MS/MS) analysis allows for protein enrichment, which aids in the identification of specific target proteins.

In the present study, we investigated characteristic glycan structures in the doxorubicin (DXR)-treated human hepatoma cell line Huh7, and further identified their target glycoproteins using iTRAQ and SSA lectin precipitation followed by LC–MS/MS. In addition, the expression levels of these proteins were confirmed using Western blotting, and their biological significance in CSC functions is discussed.

■ MATERIALS AND METHODS

Cell Culture and Cell Treatments

The human hepatoma cell line Huh7 was obtained from American Type Culture Collection (ATCC, Manassas, VA, USA) and cultured in RPMI 1640 (Sigma, St. Louis, MO, USA) medium containing 10% fetal bovine serum (Invitrogen, Carlsbad, CA, USA), supplemented with 100 units/mL penicillin G and 100 μg/mL streptomycin in a 37 °C incubator under a humidified atmosphere containing 5% CO_2. The cells were seeded into 100 mm dishes at 1×10^6 cells/dish. After 6 h, doxorubicin (DXR) (Sigma) was added to the culture medium (5 μg/mL). The cells were harvested after 48 h of exposure to DXR, and the culture media were harvested as conditioned media for the following analyses.

Lectin Microarray

Patterns of oligosaccharide structures in Huh7 cells treated with or without DXR were investigated by means of evanescent-field fluorescence-assisted lectin microarray. Forty-five types of lectins were immobilized on a glass slide in triplicate. The procedure has been described in detail, previously.[29] Briefly, total cellular proteins in phosphate buffered saline (PBS) containing 1% Triton X-100 were labeled with Cy3-succinimidyl ester (GE Healthcare, Chalfont St. Giles, U.K.) at room temperature (RT) for 1 h in the dark. Excess reagent was removed by gel filtration chromatography. The resultant Cy3-labeled protein solution was applied to a lectin microarray. After incubation at 20 °C for 15 h, the glass slide was scanned with an evanescent-field fluorescence scanner, GlycoStation (GP Biosciences Ltd., Kanagawa, Japan). All of the data were analyzed using Array Pro Analyzer version 4.5 (Media Cybernetics, Inc., Bethesda, MD, USA). The net

intensity value for each spot was calculated by subtracting the background value. The signal intensity value for each lectin was expressed as the average of the net intensity values for three spots. The signal from wheat germ agglutinin (WGA) was used to normalize the signal intensity of each lectin because binding to WGA lectin was relatively stable and similar using different cell types.

Mass Spectrometric Analysis

NanoLC–MS/MS analyses were performed on LTQ-Orbitrap XL (Thermo Fisher Scientific, Waltham, MA) equipped with nano-ESI source and coupled to Paradigm MG4 pump (Michrom Bioresources, Auburn, CA) and autosampler (HTC PAL, CTC Analytics, Zwingen, Switzerland). Peptide mixtures were separated on MagicC18AQ column (100 mm × 150 mm, 3.0 μm particle size, 300 Å, Michrom Bioresources) with a flow rate of 500 nL/min. A linear gradient of 5–30% B in 80 min, 30–95% B in 10 min, and 95% B for 4 min and finally decreased to 5% B was employed (A = 0.1% formic acid in 2% acetonitrile; B = 0.1% formic acid in 90% acetonitrile). Intact peptides were detected in the Orbitrap at 30,000 resolution. Up to three CID and HCD spectra were acquired in a data-dependent acquisition mode following each full scan (m/z, 400–1500). The mass spectrometer was operated in positive ion mode.

Preparation of Labeled Peptides for Isobaric Tags for Relative and Absolute Quantitation (iTRAQ) Analysis

Each protein sample (adjusted to 4.1 mg) was digested with 50 μg of Trypsin-TPCK Solution (Applied Biosystems, Framingham, MA, USA) at 37 °C overnight and sialylated proteins were isolated using *Sambucus sieboldiana* agglutinin (SSA) covalently linked to agarose beads (SSA-agarose) (J-Oil Mills, Inc., Tokyo, Japan). After applying to an SSA-agarose column, each sample was incubated for 6 h at 4 °C. The SSA-Agarose column was washed with 1 mL of 50 mM Tris HCl [pH 7.4] buffer five times. Bound peptides were eluted from the SSA-Agarose column using 1 mL of the elution buffer (0.2 M lactose) three times. The eluted samples were deglycosylated with glycopeptidase F. Deglycosylated peptides were desalted and labeled with iTRAQ reagents (Applied Biosystems) according to the manufacturer's instructions. Proteins from Huh7 cells, treated with or without DXR and eluted from SSA agarose, were labeled with iTRAQ reagents 114 and 115, respectively. All labeled peptide samples were mixed and fractionated as described previously.[30]

iTRAQ Data Analysis

Protein identification and quantification for iTRAQ analysis was carried out using Proteome Discoverer v.1.3 (Thermo Fisher Scientific) using the MASCOT algorithm against Swiss-Prot protein database (Swiss-Prot_2012_06 536,489 entries). Taxonomy was set to *Homo sapiens* (20,312 entries). Search parameters for peptide and MS/MS mass tolerance were 10 ppm and 0.8 Da, respectively, with allowance for two missed cleavages made from the trypsin digest. Carbamidomethylation (Cys) and iTRAQ4plex (Lys, N-terminal) were specified as static modifications, whereas deamidation (Asn, Gln), iTRAQ4plex (Tyr), and oxidation (Met) were specified as dynamic modifications in the database search. When deamidation of Asn were detected, the amino acids were considered as glycan binding site because glycopeptidase F treatment convert glycosylated Asn residue to Asp. Mascot results were filtered with the integrated Percolator based filter using a false discovery rate <1% (based on PSMs). Relative protein abundances were calculated using the ratio of iTRAQ reporter ion in the MS/MS scan. List of the

glycoproteins identified in iTRAQ analysis was represented in Supplementary Table 1.

Protein Identification by Mass Spectrometry

The gels were stained with the Silver Stain MS kit according to the manufacturer's instruction (WAKO Pure Chemical Industries, Ltd., Osaka, Japan). Protein spots in a silver-stained gel, corresponding to positive spots on Western blot membranes, were excised from the gel and digested in gel according to a previously described method,[31,32] using sequencing grade modified trypsin (Promega, Inc., Madison, WI). Digested peptides were then extracted with 5% TFA in acetonitrile (acetonitrile/DW 50:45), sonicated for 5 min and concentrated by evaporation. Dried peptides were dissolved in 0.1% TFA (v/v) and 2% acetonitrile (v/v) for subsequent LC−MS/MS analysis. NanoLC−MS/MS analyses were performed on a LTQ-Orbitrap XL mass spectrometer (Thermo Fisher Scientific) equipped with a nano-ESI source (AMR) and coupled to a Paradigm MG4 pump (Michrom Bioresources) and an autosampler (HTC PAL, CTC Analytics). A spray voltage of 1800 V was applied. The peptide mixture was separated on a Magic C18AQ column (100 μm × 150 mm, 3.0 μm particle size, 300 Å, Michrom Bioresources) with a flow rate of 500 nL/min. The linear gradient of 5% to 45% B in 30 min, 45% to 95% B in 0.1 min, and 95% B for 2 min and finally decreased to 5% B was employed (A = 0.1% formic acid in 2% acetonitrile; B = 0.1% formic acid in 90% acetonitrile). Intact peptides were detected in the Orbitrap at 60,000 resolutions. For LC−MS/MS analysis, 6 precursor ions were selected for subsequent MS/MS scans in a data-dependent acquisition mode following each full scan (m/z, 350−1500). A lock mass function was used for the LTQ-Orbitrap to obtain constant mass accuracy during gradient analysis. Peptides and proteins were identified by means of automated database search using Proteome Discoverer v.1.3 (Thermo Fisher Scientific) against human of Swiss-Prot protein database (Swiss-Prot_2012_06) with a precursor mass tolerance of 10 ppm, a fragment ion mass tolerance of 0.8 Da, and strict trypsin specificity, allowing for up to two missed cleavages. Carbamidomethylation of cysteine was set as a fixed modification, and oxidation of methionines was allowed as dynamic modifications. Raw data of MS/MS analysis was represented in Supplementary Figure 2.

Lectin Blot Analysis

Huh7 cells were quickly harvested from a 100 mm dish in ice-cold PBS. After precipitation by centrifugation at 2000 rpm for 5 min at 4 °C, the cells were resuspended in TNE buffer (10 mM Tris-HCl [pH 7.8], 1% NP40, 1 mM EDTA, and 0.15 M NaCl) containing a protease inhibitor cocktail (Roche, Mannheim, Germany) and then placed on ice for 30 min to allow solubilization. Samples were then centrifuged at 15,000 rpm for 15 min at 4 °C, and the supernatants were collected as cell lysates. Samples were quantitated using a bicinchoninic acid (BCA) assay kit (Pierce, Rockford, IL, USA).

In each experiment, duplicate samples were subjected to 8% sodium dodecyl sulfate polyacrylamide gel electrophoresis (SDS-PAGE) under reducing conditions. One gel was subjected to Coomassie Brilliant Blue (CBB) R-250 staining and another was transferred to a polyvinyl difluoride (PVDF) membrane (Millipore Corp., Billerica, MA, USA) for lectin blot analysis, using SSA, *Leukoagglutinating phytohemagglutinin* (L4-PHA), *Aleuria aurantia* lectin (AAL), and *Datura stramonium* (DSA). After blocking with PBS containing 3% bovine serum albumin (BSA) overnight at 4 °C, each membrane was incubated in 1:2500−1:10000 diluted biotinylated SSA, L4-PHA, AAL, and

DSA (J-Oil Mills, Inc., Tokyo, Japan) for 20 min at RT. The membranes were then washed three times with Tris-buffered saline containing 0.05% Tween-20 (TBST) (pH 7.4) and incubated with 1:2500 diluted avidin−peroxidase conjugates (ABC kits, Vector Res. Corp., Burlingame, CA, USA) for 20 min at RT. The membrane was again washed three times with TBST and then developed using an enhanced chemiluminescence system, Immobilon Western (Millipore), according to the manufacturer's protocol.

Immunoblot Analysis

Cell lysates and conditioned media were subjected to 8% SDS-PAGE under reducing conditions and then transferred to a PVDF membrane (Millipore). After blocking with PBS containing 5% skim milk for 1 h at RT, each membrane was incubated overnight at 4 °C with the following primary antibodies diluted 1:1000−1:5000: anti-HYOU1 (Abnova, Taipei, Taiwan), anti-P4HA1 (Abnova, Taipei City, Taiwan), anti-LAMP1 (Abcam Inc., Cambridge, MA, USA), anti-LAMP2 (Santa Cruz Biotechnology Inc., Santa Cruz, CA, USA), antibeta-galactosidase (Santa Cruz Biotechnology), antifetuin-A (Santa Cruz Biotechnology), or anti-β-actin (Cell Signaling, Beverly, MA, USA) for 60 min at RT. The dilution ratios for these antibodies ranged from 1:1000 to 1:5000. The membranes were then washed three times with Tris-buffered saline containing 0.05% Tween-20 (TBST) (pH 7.4) and incubated with 1:5000 diluted horseradish peroxidase conjugated with the appropriate secondary antibody for 30 min at RT. The membranes were again washed three times and developed using an Immobilon Western (Millipore).

Lectin Precipitation

Extracted protein (100 μg) was incubated with 40 μL of SSA-agarose overnight with shaking at 4 °C. Precipitated proteins were washed in 50 mM Tris HCl [pH 7.4] and then boiled in SDS sample buffer. Ten microliters of precipitated proteins were subjected to 8% SDS-PAGE. The gel was stained with Silver Stain MS Kits (Wako, Osaka, Japan). Protein bands were excised from the gel and digested with sequencing grade trypsin (Promega) as described previously.[33]

Neuraminidase/N-Glycanase Treatments

The extracted proteins (100 μg) were incubated overnight at 37 °C with 200 mU/mL of neuraminidase (Roche, Nutley, NJ, USA) in 50 mM AcOH buffer [pH 5.5] containing 4 mM CaCl$_2$ and 100 μg/mL BSA. In addition, 100 μg of the extracted proteins were incubated with glycopeptidase F (Takara Bio Inc., Otsu, Japan) according to the manufacturer's protocol. The cell lysates were subsequently boiled in SDS-PAGE sample buffer, electrophoresed on 8% SDS PAGE, and then transferred onto a PVDF membrane (Millipore). After blocking with TBST containing 5% skim milk at 4 °C overnight, Western blot analysis for fetuin-A was performed using antifetuin-A antibody.[34] Briefly, 1:5000 diluted antifetuin-A was incubated in TBST buffer containing 5% skim milk for 1 h at RT. After washing the membrane three times with TBST, it was incubated for 1 h at RT with the secondary antibody, horseradish peroxidase-conjugated antirabbit-IgG (Promega), diluted 1:5000. It was again washed three times and developed with an Immobilon Western (Millipore).

Immunofluorescence Confocal Microscopy

Huh7 cells were seeded in 35 mm dishes at 3 × 10^5 cells/dish. After 6 h, DXR was added to the culture medium (5 μg/mL). After 48 h of exposure to DXR, cells were washed once in PBS
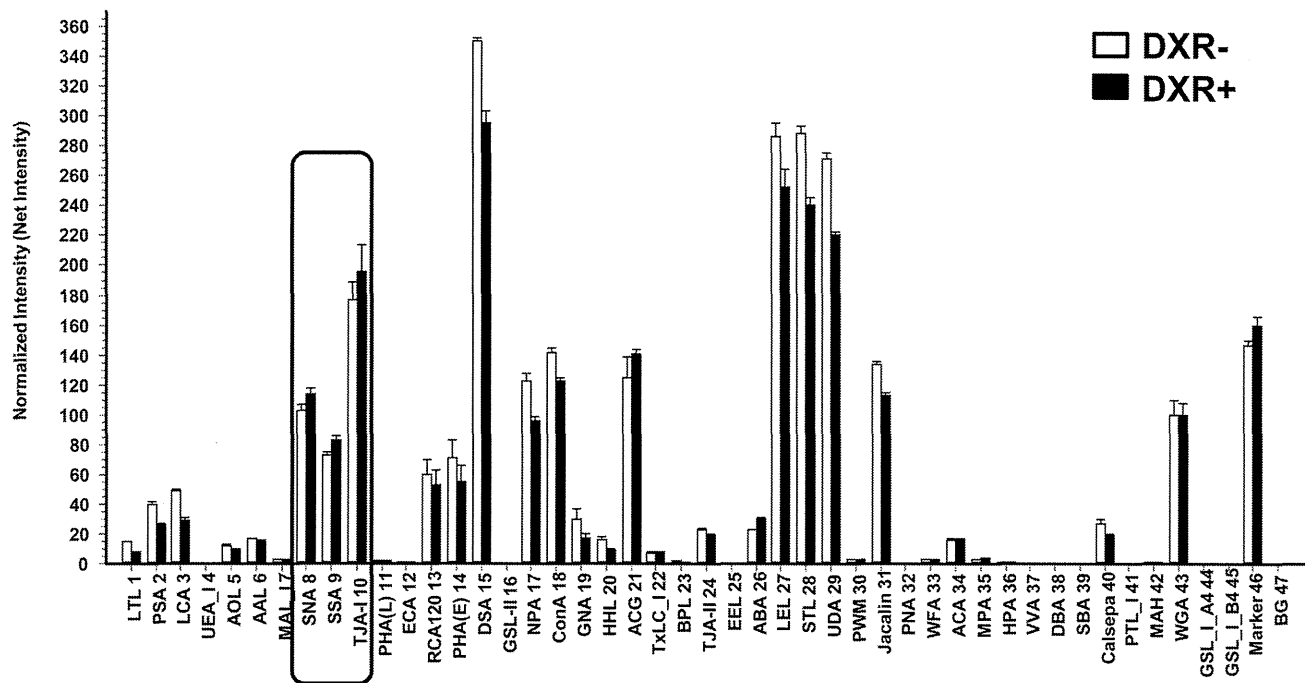
Figure 1. Lectin microarray analysis. Total cellular proteins of Huh7 cells treated with or without doxorubicin were analyzed three times using lectin microarray. Twenty-five nanogram aliquots of Cy3-labeled proteins were applied to each lectin microarray. The fluorescence intensity of each lectin was normalized to the intensity of WGA staining. All data are represented as mean ± standard deviations (SD). The Wilcoxon test was used to assess any significant differences in variables. There were significant increases in the intensities of SNA, SSA, and TJA-1 after doxorubicin treatment (DXR+) compared with the intensities in the absence of doxorubicin treatment (DXR−) ($P < 0.05$).

Table 1. Expression Profile of Sialylated Proteins in Doxorubicin-Treated Huh7 Cells, Obtained from iTRAQ Analysis

Swiss-Prot accession number	sequence	description	gene symbol	site	115/114	115/114 count	115/114 variability [%]
Q9Y4L1	VFGSQNLTTVK	hypoxia up-regulated protein 1	HYOU1	N515	7.137	1	
P13674	DMSDGFISNLTIQR	prolyl 4-hydroxylase subunit alpha-1	P4HA1	N367	4.857	1	
P11279	SGPKNMTFDLPSDATVVLNR	lysosome-associated membrane glycoprotein 1	LAMP1	N562, N76	3.796	1	
O60568	SAEFFNYTVR	procollagen-lysine, 2-oxoglutarate 5-dioxygenase 3	PLOD3	N63	2.848	1	
O60568	EQYIHENYSR	procollagen-lysine, 2-oxoglutarate 5-dioxygenase 3	PLOD3	N548	2.347	1	
P11142	VEIIANDQGNR	heat shock cognate 71 kDa protein	HSPA8	N31	2.152	1	
P16278	NNVITLNITGK	beta-galactosidase	GLB1	N458, N464	1.963	1	
P11279	NMTFDLPSDATVVLNR	lysosome-associated membrane glycoprotein 1	LAMP1	N62, N76	1.890	1	
Q92508	ELYNGTADITLR	piezo-type mechanosensitive ion channel component 1	PIEZO1	N2294	1.852	1	
P11279	ENTSDPSLVIAFGR	lysosome-associated membrane glycoprotein 1	LAMP1	N84	1.836	2	6.0
Q86VZ4	SSDNVSVTVLR	low-density lipoprotein receptor-related protein 11	LRP11	N291	1.806	2	8.6
P19022	SNISILR	cadherin-2	CDH2	N692	1.804	1	
P13473	AASTYSIDSVSFSYNTGDNTTFPDAEDK	lysosome-associated membrane glycoprotein 2	LAMP2	N257	1.699	1	
Q5ZPR3	TALFPDLLAQGNASLR	CD276 antigen	CD276	N104	1.697	1	
P11047	TLAGENQTAFEIEELNR	laminin subunit gamma-1	LAMC1	N1223	1.696	1	
Q5ZPR3	QLVHSFAEGQDQGSAYANR	CD276 antigen	CD276	N309	1.634	1	
P13473	VQPFNVTQGK	lysosome-associated membrane glycoprotein 2	LAMP2	N356	1.614	2	12.5
P56199	VYVYALNQTR	integrin alpha-1	ITGA1	N532	1.611	1	

and fixed with methanol for 10 min at −20 °C, followed by blocking with PBS containing 1% BSA for 1 h at RT. The cells

were then incubated overnight at 4 °C with the mouse antifetuin-A antibody (Santa Cruz Biotechnology) and rabbit antialbumin

4872

antibody (Rockland Immunochemicals, Gilbertsville, PA, USA). Fluorescein isothiocyanate (FITC)-conjugated SSA (J-Oil Mills, Inc., Tokyo, Japan) was incubated for 2 h at RT. Primary antibody binding was detected with Alexa-488 antimouse IgG or Alexa-546 antirabbit IgG (Invitrogen). Finally, the cells were washed three times for 2 min with PBS. Staining was evaluated using confocal microscopy.

Statistical Analysis

Statistical analyses were conducted using JMP Pro 10.0 software (SAS Institute Inc., Cary, NC, USA). Variables in lectin array analyses were expressed as the mean ± standard deviation (SD). The Wilcoxon test was used to assess any significant differences in variables. Differences were considered statistically significant at $P < 0.05$.

RESULTS

## Glycan Profiling of Huh7 Cells Treated with or without DXR Using Lectin Microarray

First, we determined the DXR IC_{50} concentration in Huh7 cells treated with DXR for 48 h, using the WST assay (Nacalai Tesque, Kyoto, Japan) (data not shown). Huh7 cells were treated with the IC_{50} concentration of DXR (5 μg/mL) for 48 h, and then Cy3-labeled proteins derived from these cells were subjected to lectin microarray analysis (Figure 1). Interestingly, the intensities of three sialylated glycan-recognizing lectins (SNA, SSA, and TJA-1) among 43 lectins were significantly higher in DXR-treated cells than in untreated cells. This finding is very similar to that of our previous study, which demonstrated that hepatic CSCs (CD133 and CD13 double-positive Huh7 cells) highly expressed sialylated glycans.[16] In this previous study, we also demonstrated that SSA lectin could be used as a tool for isolating CSCs. Unexpectedly, binding to the lectins PSA and LCA was slightly decreased in DXR-treated cells. Both PSA and LCA lectins recognize $\alpha 1-6$ core fucosylation, which is involved in carcinogenesis. Changes in the branching formation of N-glycans, as judged by binding to L4-PHA lectin, were not observed in Huh7 cells treated with DXR.

Sialylated Protein Expression Profile of Huh7 Cells Treated with or without DXR

To identify target glycoproteins that show increased sialylation upon DXR treatment, iTRAQ analysis was performed. Total cell lysates from Huh7 cells treated with or without DXR were trypsinized and applied to a SSA-agarose column. Subsequently, captured sialylated glycopeptides were deglycosylated with glycopeptidase F and labeled with a specific isobaric iTRAQ reagent. A total of 191 proteins were identified with this analysis. Among these, we have listed glycoproteins that showed more than 1.6-fold expression in DXR-treated Huh7 cells as compared with that in DXR-untreated Huh7 cells (Table 1).

## Western Blot Analysis of Glycoprotein Listed by iTRAQ Analysis

To further verify the changes in the glycoproteins listed in Table 1, we selected four proteins [hypoxia up-regulated protein 1 (HYOU1), prolyl 4-hydroxylase subunit alpha-1 (P4HA1), lysosomal-associated membrane glycoprotein 1 (LAMP1), and LAMP2], which are known to be abundantly glycosylated and associated with cancer, for validation using Western blotting (Figure 2). The expression levels of HYOU1 and P4HA1 showed no significant differences between Huh7 cells with or without DXR treatment. This indicates that the sialylation levels of these proteins increased with DXR treatment and total protein levels were not changed. In contrast, both LAMP1 and LAMP2 protein levels were slightly increased in DXR-treated Huh7 cells.
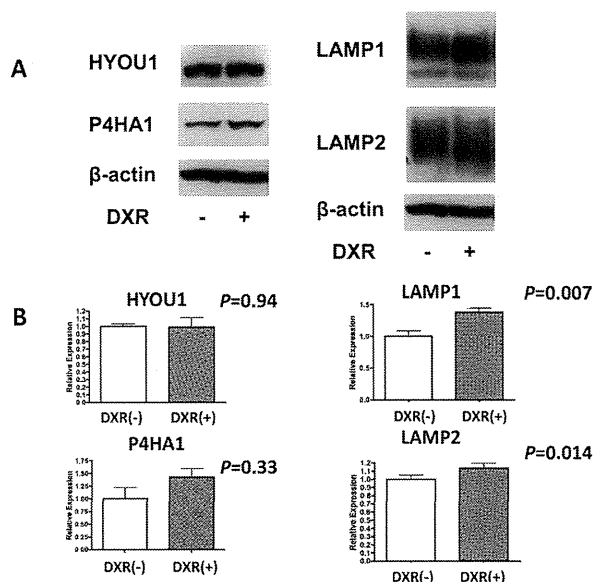
Figure 2. Western blot analyses of HYOU1, P4HA1, LAMP1, and LAMP2. (A) Twenty-five micrograms (HYOU1 and P4HA1), 10 μg (LAMP1 and β-actin), and 2.5 μg (LAMP2) of total cellular proteins were electrophoresed on 8% polyacrylamide gels, and Western blot analyses were performed. β-actin was used as the control. (B) Expression level of each protein band was determined by ImageJ64 software for three independent blots, and statistical analysis was performed by Wilcoxon test. Each result represented the mean ± SD.

Increase in Sialylation of 70 kDa Proteins in DXR-Treated Huh7 Cells

Next, we performed lectin blot analysis to determine changes in sialylation in each protein band in DXR-treated Huh7 cells. Very interestingly, dramatic increases in sialylation in approximately 70 kDa proteins were observed (Figure 3A). While other bands
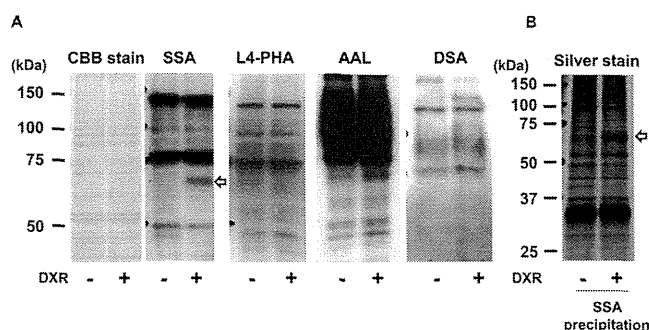
Figure 3. Lectin blot analyses and SSA precipitation of Huh7 cells treated with or without doxorubicin. (A) Lectin blot analyses using SSA, AAL, L4-PHA, and DSA. (B) Proteins were captured by SSA-agarose bead complexes, followed by 10% SDS-PAGE analysis with silver staining. The arrows indicate specifically sialylated bands. These data were results from 3–5 independent experiments.

in the SSA lectin blot were slightly increased or decreased in DXR-treated cells, the 70 kDa proteins were very prominent. Therefore, the protein levels of these 70 kDa proteins might be increased upon DXR treatment. Mechanisms that can increase sialylation in glycoproteins include increased branching, increased presence of Lewis structures, and extension of lactosamine structure repeats. L4-PHA, AAL, and DSA can recognize these glycan structures, respectively. Therefore, we examined these lectin blot analyses. The 70 kDa band was not

detected in other lectin blot analyses, although a significant increase was observed in AAL lectin blot analysis (Figure 3A). The increase in the intensity of the 70 kDa band in the DXR-treated cells in the AAL blot indicates an increased presence of Lewis structures in some glycoproteins. To capture this sialylated glycoprotein at 70 kDa, SSA precipitation was performed (Figure 3B). As shown in Figure 3B, approximately 70 kDa sialylated glycoproteins were identified using SSA-agarose precipitation followed by silver staining. Next, the 70 kDa protein spot was digested with trypsin, and the extracted peptides were analyzed using LC–MS/MS. The spectra thus acquired were searched against the Swiss-Prot database with the aid of the MASCOT search engine. In this manner, we identified five proteins as candidate sialylated glycoproteins (Table 2).

Table 2. Sialylated 70 kDa Proteins Identified by LC–MS/MS

Swiss-Prot accession no.	protein	peptide matching	protein coverage (%)
P16278	beta-galactosidase	12	11.23
P02765	alpha-2-HS-glycoprotein (fetuin-A)	8	5.45
Q02413	desmoglein-1	2	0.95
Q9NPR9	protein GPR108	2	2.03
P11279	lysosome-associated membrane glycoprotein 1	1	2.64

Evaluation of the 70 kDa Sialylated Proteins in DXR-Treated Huh7 Cells by Western Blot

To evaluate the 70 kDa sialylated proteins listed in Table 1, Western blotting was performed. Because of their large hit numbers in LC–MS/MS analysis, we focused on fetuin-A and beta-galactosidase. Although the protein expression of beta-galactosidase was slightly increased in DXR-treated Huh7 cells, the protein expression of beta-galactosidase obtained by SSA precipitation was much greater in DXR-treated Huh7 cells (Figure 4A). This result indicates that the sialylation levels of beta-galactosidase increased with DXR treatment. Next, Western blot analyses of alpha-2-HS-glycoprotein (fetuin-A) were performed. Although the protein expression of fetuin-A in total cell lysate was lower in DXR-treated Huh7 cells, the protein expression of fetuin-A obtained by SSA precipitation was significantly higher in DXR-treated Huh7 cells (Figure 4B). Furthermore, the molecular weight of fetuin-A was higher in DXR-treated Huh7 cells. These results indicate that oligosaccharide structures of fetuin-A are completely different between DXR-treated and untreated Huh7 cells. Additionally, the molecular weight of fetuin-A in the conditioned medium was almost the same between DXR-treated and untreated cells, which was consistent with the sialylated fetuin-A band (70 kDa) observed in cell lysates treated with DXR (Figure 4C). We found that sialylated fetuin (70 kDa) was barely observed in untreated cell lysate and almost all of the 70 kDa fetuin was secreted into the medium in the absence of DXR treatment. In order to determine whether the changes in molecular weight of fetuin-A were due to glycosylation/sialylation, the total cell lysates of DXR-treated and untreated Huh7 cells were incubated with 200 mU/mL neuraminidase, which specifically cleaves terminal sialic acid residues. A decrease of the molecular weight of fetuin-A was observed following neuraminidase treatment, suggesting that sialylation in fetuin-A was increased upon DXR treatment (Figure 4D). Next, to determine whether the changes in fetuin-A bands were dependent on N-glycosylation, cell lysates were treated with 20 mU/mL glycopeptidase F, which removes most complex type N-linked carbohydrates from

glycoproteins. As expected, the fetuin-A band was decreased following this treatment (Figure 4D).

Localization of Fetuin-A in Huh7 Cells Treated with DXR

To examine the localization of fetuin-A in DXR-treated Huh7 cells, an immunofluorescence study was performed. Cells were stained with antifetuin-A antibody (Figure 5A,B), and anti-albumin antibody, which served as a nonglycosylated secretory protein control (Figure 5A) and SSA (Figure 5B). Although the expression of fetuin-A was lower in DXR-treated Huh7 cells than in untreated cells, colocalization of fetuin-A and albumin were observed in DXR-treated and untreated cells. In contrast, the localization of SSA changed dramatically in DXR-treated cells (Figure 5B). The localization of these signals was altered in DXR-treated cells from a perinuclear pattern to a scatter pattern in the cytoplasm. SSA and fetuin-A were not colocalized in DXR-untreated cells, but a few DXR-treated cells showed colocalization of SSA and fetuin-A (Figure 5B).

■ DISCUSSION

In the present study, to identify target glycoproteins for SSA lectin, we first used iTRAQ systems with SSA-agarose capture. However, the amounts of cellular proteins that could be isolated using CD133 antibody and SSA lectin were too small for proteomic analyses. Therefore, we used the anticancer drug DXR. Theoretically, treatment with DXR at its IC_{50} can concentrate CSCs. Lectin array analyses showed increased binding to SSA, SNA, and TJA-1 in DXR-treated Huh7 cells. Similar results were obtained in CD133 and CD13 double-positive CSCs derived from Huh7 cells.[16] These findings suggest that Huh7 cells treated with DXR display similar characteristics to CSCs. SSA, SNA, and TJA-1 recognize terminal $\alpha2$, 6-sialic acid residues. We speculate that this increased sialylation in DXR-treated Huh7 cells might have potential benefits for the survival of anticancer drug-treated cells. To identify those glycoproteins that are targets for sialylation, iTRAQ analysis was performed. Of the 19 candidate glycoproteins we identified, concentration of HYOU1 was much greater than those of the other glycoproteins. HYOU1 plays an important role in hypoxia/ischemia and angiogenesis. HYOU1 is overexpressed in invasive breast cancer, and its overexpression appears to be associated with poor prognosis.[35] A high score in iTRAQ analyses using SSA agarose capture may indicate one of two possibilities: an increase in the glycoprotein level itself or an increase in sialic acid levels in a specific glycoprotein. Protein levels remain unchanged in the case of HYOU1 (Figure 2). Although we would have liked to perform immunoprecipitation followed by SSA lectin blotting, the antibody for immunoprecipitation was not available. We predict that sialic acid increases in HYOU1 in DXR-treated Huh7 cells. The next high score in iTRAQ analysis was that of P4HA1. P4HA1 plays a central role in collagen synthesis. P4HA1 has also been shown to be expressed in hepatocellular carcinoma tissue. In contrast, the protein expression levels of LAMP1 and LAMP2 were increased with DXR treatment. LAMP1 and LAMP2 are localized primarily in the periphery of lysosomes and are recognized as major constituents of the lysosomal membrane.[36] It is well-known that these molecules are among the most heavily glycosylated cellular proteins, with approximately 50% of their mass being carbohydrates. Therefore, these proteins could be captured by an SSA-agarose column and detected using iTRAQ analysis. Since these 4 glycoproteins are associated with cancer progression as well as metastasis, increases in sialic acid content
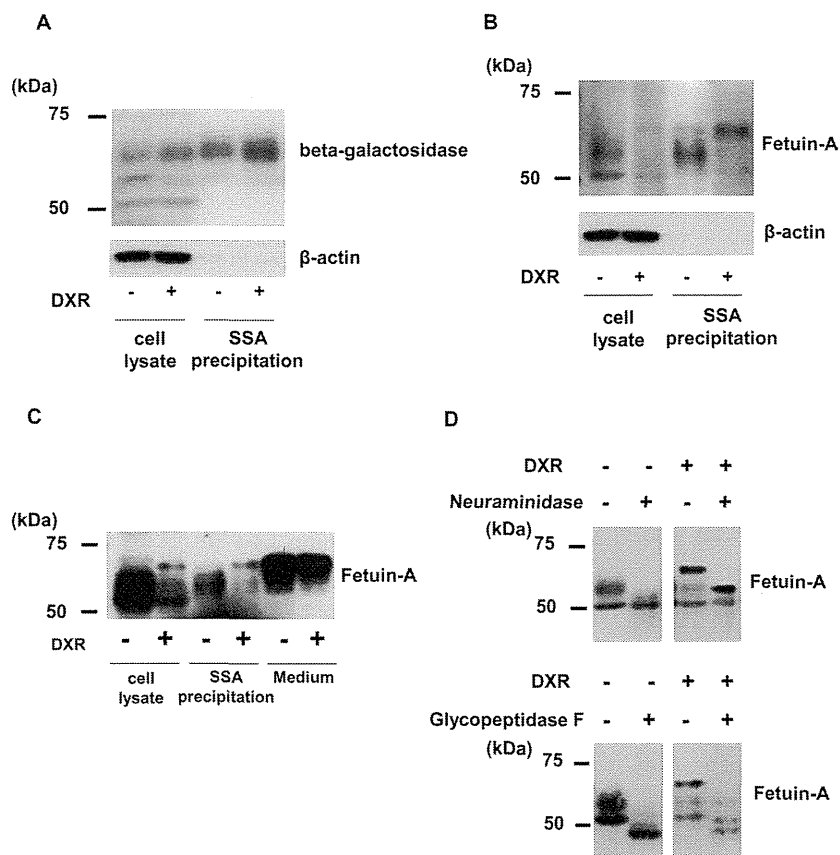
Figure 4. Evaluation of 70 kDa sialylated proteins in Huh7 cells treated with doxorubicin with Western blotting. (A) Ten micrograms of cell lysate and total cellular proteins obtained from lectin precipitation (50 μg) were electrophoresed on 8% acrylamide gels, and Western blot analyses of beta-galactosidase were performed. (B) Western blotting analysis of fetuin-A was performed. (C) Western blotting analysis of fetuin-A from Huh7 cell lysates (30 μg) and conditioned media (1 μL) in the presence or absence of DXR treatment. (D) Cell lysates were treated with neuraminidase or glycopeptidase F at 37 °C overnight. The lysates were then subjected to 8% SDS-PAGE analysis. These data were results from 3 independent experiments.

in these proteins can change biological characteristics, including cancer stemness.

Next, we conducted an SSA lectin blot analysis to determine total/partial increases in sialic acid content in DXR-treated Huh7 cells. Surprisingly, proteins approximately 70 kDa in mass were specifically sialylated. From LC−MS/MS analyses, we identified five proteins that were not identified by iTRAQ analysis, with the exception of LAMP1. Fetuin-A (predicted molecular weight: 38 kDa), GPR108 (predicted molecular weight: 60 kDa), LAMP1 (predicted molecular weight: 45 kDa), and LAMP2 (predicted molecular weight: 45 kDa) are abundantly glycosylated. In our study, 70 kDa fetuin-A was heavily sialylated. Therefore, the band sizes of fetuin-A, GPR108, LAMP1, and LAMP2 were heavier than the predicted molecular weights. In addition, the predicted size of beta-galactosidase is about 116 kDa, but the alternatively spliced variant of beta-galactosidase was reported to be about 67 kDa.[37] Desmoglein-1 (predicted molecular weight: 112 kDa) would be cleaved by DXR-activated proteases. The reason why these proteins were not identified by iTRAQ is likely due to the analysis method of iTRAQ. Because proteins are cleaved into peptides in iTRAQ analysis, the steric structures of each protein is not reflected in iTRAQ analysis. In contrast, the steric structures of each protein and the site of N-glycan attachment are necessary in SSA precipitation analysis. These differences between iTRAQ and SSA precipitation are likely the reason for the different results seen in our study.

In LC−MS/MS analysis, we focused on beta-galactosidase and fetuin-A because of their predominantly large hit numbers.

Beta-galactosidase (lysosomal hydrolase) cleaves the terminal beta-galactose from glycoconjugates. It is reported that anticancer drug treatment induces a senescence-like phenotype, and senescent cells are characterized by the appearance of senescence-associated beta-galactosidase.[38] Therefore, increases in sialic acid in beta-galactosidase in DXR-treated Huh7 cells are very interesting. Another glycoprotein, identified as a 70 kDa sialylated glycoprotein, was fetuin-A. Fetuin-A is well-known as a heavily sialylated glycoprotein with both N-linked and O-linked carbohydrate side chains.[39,40] Although various previous reports have discussed the biological functions of fetuin-A,[41,42] no studies have demonstrated differences in fetuin-A functions due to glycosylation differences. Asialofetuin-A is well-known to bind easily to galectin-3, while sialylated fetuin (sialofetuin) is reported to have no binding ability to galectin-3.[43,44] These biological differences would contribute to the functional diversity of variously glycosylated fetuin-A.

Neuraminidase treatment decreases the molecular weight of fetuin-A in DXR-treated Huh7 cells, and the lowered molecular weight was consistent with that of fetuin-A in DXR-untreated Huh7 cells, suggesting that fetuin-A was heavily sialylated in DXR-treated Huh7 cells. The question arises as to why this sialylated fetuin-A was not secreted into the conditioned medium. Therefore, we performed immunocytochemical analysis using confocal microscopy. Most of the fetuin-A was colocalized with albumin in DXR-treated cells compared to untreated cells, indicating that the secreted proteins were in the same endosome as during DXR treatment. A previous study
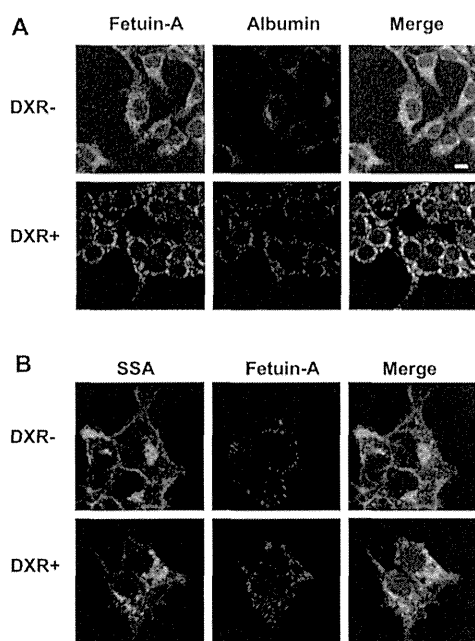
Figure 5. Localization of fetuin-A in Huh7 cells treated with doxorubicin. Immunocytochemical analyses were performed in Huh7 cells treated with or without DXR. After fixation of the cells, staining signals were visualized by laser scanning confocal microscopy. (A) Fetuin-A was visualized by Alexa-488-labeled immunostaining (green), albumin was visualized by Alexa-546-labeled immunostaining (red). (B) SSA was visualized by FITC labeling (green), and fetuin-A was visualized by Alexa-546-labeled immunostaining (red). The magnification is ×120. The bar indicates 10 μm. These data were results from 3 independent experiments.

showed that DXR induced apoptosis at a high dose (IC_{90}) but induced autophagy at a low dose (IC_{50}).[45] However, fetuin-A was not located in either the lysosome or the autophagosome (data not shown). Next we examined immunostaining of SSA to detect sialylated proteins. Surprisingly, SSA staining was dramatically changed, and a few cells showed colocalization of fetuin-A and SSA in DXR-treated cells. These results indicate that a small amount of sialylated fetuin-A remained inside the cell in DXR-treated cells. In general, fetuin-A is known as a highly sialylated serum protein.[46] Most sialylated fetuin-A might be promptly secreted to the conditioned medium (Figure 4C). In contrast, a small amount of sialylated fetuin-A remained inside the cell in DXR-treated cells. Further studies should be performed using sialyltransferase knockout or knockdown cells to evaluate the relationship between sialylation and the localization of glycoproteins, especially that of fetuin-A in anticancer drug treated cells. Since sialylation is a glycomarker for stem cells,[16,47] changes in the localization of sialylated proteins in CSCs might be involved in stem cell biology.

ASSOCIATED CONTENT

Supporting Information

Proliferation of CD133 positive Huh7 cells (SSA positive (+) or negative (−)) under 5-FU treatment. Raw data of MS/MS analysis. List of the glycoproteins identified in iTRAQ analysis. This material is available free of charge via the Internet at http://pubs.acs.org.

AUTHOR INFORMATION

Corresponding Author

*(E.M.) Tel/Fax: +81-6-6879-2590. E-mail: emiyoshi@sahs. med.osaka-u.ac.jp.

ABBREVIATIONS

CSCs, cancer stem cells; DXR, doxorubicin; SSA, *Sambucus sieboldiana* agglutinin; SNA, *Sambucus nigra* lectin; TJA-1, *Tricosanthes japonica* agglutinin-1; PSA, *Pisum sativum* agglutinin; LCA, *Lens culinaris* agglutinin; WGA, Wheat germ agglutinin; L4-PHA, *Leukoagglutinating phytohemagglutinin*; AAL, *Aleuria aurantia* lectin; DSA, *Datura stramonium agglutinin*; iTRAQ, isobaric tags for relative and absolute quantitation; HYOU1, hypoxia up-regulated protein 1; P4HA1, prolyl 4-hydroxylase subunit alpha-1; LAMP1, lysosomal-associated membrane glycoprotein 1

REFERENCES

(1) Reya, T.; Morrison, S. J.; Clarke, M. F.; Weissman, I. L. Stem cells, cancer, and cancer stem cells. *Nature* 2001, 414 (6859), 105−11.

(2) Ailles, L. E.; Weissman, I. L. Cancer stem cells in solid tumors. *Curr. Opin. Biotechnol.* 2007, 18 (5), 460−6.

(3) Mertins, S. D. Cancer stem cells: a systems biology view of their role in prognosis and therapy. *Anticancer Drugs* 2014, 25 (4), 353−67.

(4) Dean, M.; Fojo, T.; Bates, S. Tumour stem cells and drug resistance. *Nat. Rev. Cancer* 2005, 5 (4), 275−84.

(5) Bao, S.; Wu, Q.; McLendon, R. E.; Hao, Y.; Shi, Q.; Hjelmeland, A. B.; Dewhirst, M. W.; Bigner, D. D.; Rich, J. N. Glioma stem cells promote radioresistance by preferential activation of the DNA damage response. *Nature* 2006, 444 (7120), 756−60.

(6) Malik, B.; Nie, D. Cancer stem cells and resistance to chemo and radio therapy. *Front. Biosci., Elite Ed.* 2012, 4, 2142−9.

(7) Baumann, M.; Krause, M.; Thames, H.; Trott, K.; Zips, D. Cancer stem cells and radiotherapy. *Int. J. Radiat. Biol.* 2009, 85 (5), 391−402.

(8) Haraguchi, N.; Ishii, H.; Mimori, K.; Tanaka, F.; Ohkuma, M.; Kim, H. M.; Akita, H.; Takiuchi, D.; Hatano, H.; Nagano, H.; Barnard, G. F.; Doki, Y.; Mori, M. CD13 is a therapeutic target in human liver cancer stem cells. *J. Clin. Invest.* 2010, 120 (9), 3326−39.

(9) Zhu, Z.; Hao, X.; Yan, M.; Yao, M.; Ge, C.; Gu, J.; Li, J. Cancer stem/progenitor cells are highly enriched in CD133+CD44+ population in hepatocellular carcinoma. *Int. J. Cancer* 2010, 126 (9), 2067−78.

(10) Yang, Z. F.; Ho, D. W.; Ng, M. N.; Lau, C. K.; Yu, W. C.; Ngai, P.; Chu, P. W.; Lam, C. T.; Poon, R. T.; Fan, S. T. Significance of CD90+ cancer stem cells in human liver cancer. *Cancer Cell* 2008, 13 (2), 153−66.

(11) Al-Hajj, M.; Wicha, M. S.; Benito-Hernandez, A.; Morrison, S. J.; Clarke, M. F. Prospective identification of tumorigenic breast cancer cells. *Proc. Natl. Acad. Sci. U.S.A.* 2003, 100 (7), 3983−8.

(12) Kojima, K.; Musch, M. W.; Ren, H.; Boone, D. L.; Hendrickson, B. A.; Ma, A.; Chang, E. B. Enteric flora and lymphocyte-derived cytokines determine expression of heat shock proteins in mouse colonic epithelial cells. *Gastroenterology* 2003, 124 (5), 1395−407.

(13) Ding, W.; Mouzaki, M.; You, H.; Laird, J. C.; Mato, J.; Lu, S. C.; Rountree, C. B. CD133+ liver cancer stem cells from methionine adenosyl transferase 1A-deficient mice demonstrate resistance to transforming growth factor (TGF)-beta-induced apoptosis. *Hepatology* 2009, 49 (4), 1277−86.

(14) Fuster, M. M.; Esko, J. D. The sweet and sour of cancer: glycans as novel therapeutic targets. *Nat. Rev. Cancer* 2005, 5 (7), 526−42.